

**Mathematical Modelling of Grid Connected Fixed-Pitch
Variable-Speed Permanent Magnet Synchronous
Generators for Wind Turbines**

By

Zaiming Fan

A thesis submitted in partial fulfilment for the requirements of the degree of
MSc (by Research) at the University of Central Lancashire

June 2012

荣耀归于全能的上帝

献给我太太, 儿子与家人

感谢他们的支持与信任

我爱你们

Glory be to Almighty God

Dedicated to my wife, my son and my parents

For their support and trust, many thanks

I love all of you

Abstract

This project develops the mathematical model of a 10kW permanent magnet synchronous generator (PMSG), which is designed for a fixed-pitch variable-speed wind turbine, and its corresponding simulation model for the control of the PMSG for grid connection using MATLAB/Simulink. The model includes sub-modules, such as a model of the wind speed, a model of the PMSG, a model of the rectifier circuit, a model of the boost chopper circuit, a model of the space vector pulse width modulation (SVPWM) inverter, and a model of the power grid voltage sag detection for low voltage ride through (LVRT). The rectifier is a 3-phase uncontrolled diode full-bridge circuit. The boost chopper circuit offers a direct current (DC) power supply with constant voltage for the inverter. Sampled signals of instantaneous 3-phase voltage (from the power grid) to obtain the phase angle, frequency and amplitude, are used to generate SVPWM signals to control the inverter's output. In the model of the power grid voltage sag detection, a novel direct-quadrature (DQ) transformation is introduced to detect the voltage sag of the power grid.

This thesis systematically analyses the mathematical model along with its sub-modules, and creates simulation models using MATLAB/Simulink. The simulation results demonstrate that both the mathematical model and simulation model are correct, and the parameters of the generator output are synchronised with the main grid.

Contents

Acknowledgements.....	VI
List of Abbreviations	VII
List of Figures.....	VIII
List of Tables	XI
List of Symbols	XII
Chapter 1 Introduction.....	1
1.1 Background introduction.....	1
1.2 Aims and objectives	2
1.3 The framework of system	3
1.4 Structure of thesis.....	4
Chapter 2 Literature Review	6
2.1 Wind energy conversion system modelling	6
2.2 Wind turbine control for grid connection.....	6
2.2.1 Direct-coupled generator grid connection.....	7
2.2.2 Doubly-fed induction generator (DFIG) grid connection	8
2.2.3 Fully rated converter grid connection	9
2.2.4 AC/DC Rectifier and DC/ DC converter	10
2.2.5 Inverters for grid connection.....	13
2.3 Summary	14
Chapter 3 PMSG Modelling for Variable-Speed Wind Turbine.....	15
3.1 Introduction to variable-speed wind turbine with PMSG	15

3.2	Wind turbine aerodynamic characteristics	17
3.3	Mathematical modelling of PMSG	18
3.4	Mathematical inverse Park and Clarke transforms	20
3.5	Modelling PMSG with MATLAB/Simulink	21
3.5.1	Simulation of wind turbine rotor power coefficient.....	21
3.5.2	Simulation of wind turbine generator power output	22
3.5.3	PMSG Simulation	23
3.6	Summary	25
Chapter 4 AC/DC Rectifier and DC/DC Boost Circuits		26
4.1	Introduction	26
4.2	Introduction of rectifier circuit.....	26
4.2.1	Diode rectifier bridge VSCs.....	27
4.2.2	Back-to-back VSCs.....	28
4.3	DC to DC converter	29
4.3.1	Step-down (Buck) converter	29
4.3.2	Step-up (Boost) converter	31
4.4	Design of rectifier with closed-loop boost chopper	33
4.5	Modelling the rectifier with closed-loop boost chopper using MATLAB/Simulink	34
4.6	The simulation results	35
4.7	Summary	39
Chapter 5 Inverter Modelling		40

5.1	Introduction	40
5.2	The SVPWM algorithm	40
5.2.1	The principle of SVPWM	41
5.2.2	Clarke Transform	45
5.2.3	Identification	46
5.2.4	Calculate firing time for IGBT switches.....	48
5.2.5	The over modulation	49
5.2.6	The principle of pulse width modulation.....	49
5.2.7	Carrier-wave of SVPWM.....	51
5.3	Modelling SVPWM using MATLAB/Simulink	52
5.4	Summary	58
Chapter 6	Voltage Sag Detection	59
6.1	Low Voltage Ride Through	59
6.2	Overview on power grid voltage sag detection methods	61
6.3	The mathematical model of a novel grid voltage sag detection.....	64
6.3	Modelling of voltage sag detection	67
6.4	The simulation results	67
6.5	Summary	71
Chapter 7	Conclusion and Future Works.....	73
7.1	Conclusion	73
7.2	Future works	74
References	75	

Appendix-A	10kW case study wind turbine specification	78
Appendix-B	C_p vs λ.....	79
Appendix-C	PMSG parameters	82
Appendix-D	C Program for S-Builder filter	84

Acknowledgements

First of all, I am so proud to be a student of Professor Xiongwei Liu, who is my director of study. I am very grateful to his careful and generous guidance, and helps during my period of study.

I also would like to express my gratitude to my second and third supervisors Dr. Maizura Mokhtar and Dr. Javad Yazdani for their technical discussions and suggestions during every stage of my study.

With great pleasure, I would like to thank my friend Michael Peak and his wife Hui Zhang for their helps. I also thank Dr. Akanbi Oyebanji, Dr. Ruitao Peng, and Xinzi Tang, for going through this thesis.

My thanks go to all research colleagues in KM001, CM222 and CM225 for harmonious atmosphere.

Finally, I would like to express my gratitude to the authority and all members of staff at the University of Central Lancashire for the support and opportunity they provided for me to be a student of the institution. I am proud of you all.

List of Abbreviations

AC	Alternating Current
BWEA	British Wind Energy Association
CCM	Continuous Current Mode
CSI	Current Source Inverter
DC	Direct Current
DCM	Discontinuous Current Mode
DES	Distributed Energy Resource
DFIG	Doubly-Fed Induction Generator
DQ	Direct Quadrature
DSP	Digital Signal Processor
DTC	Direct Torque Control
EMF	Electromotive force
FPGA	Field Programmable Gate Array
IGBT	Insulated Gate Bipolar Transistor
LVRT	Low Voltage Ride Through
MCU	Micro Control Unit
MOSFET	Metal-Oxide-Semiconductor Field-Effect Transistor
MPPT	Maximum Power Point Tracking
PFC	Power Factor Correction
PMSG	Permanent Magnet Synchronous Generator
PWM	Pulse Width Modulation
RMS	Root Mean Square
SVPWM	Space Vector Pulse Width Modulation
VSC	Voltage Source Converter
VSI	Voltage Source Inverter

List of Figures

Figure 1- 1 The system framework	4
Figure 2- 1 Schematics of a fixed-speed wind turbine.....	8
Figure 2- 2 The typical configuration of DFIG wind turbine	9
Figure 2- 3 Fully rated converter grid connection	10
Figure 2- 4 Wind turbine PMSG with back-to-back converter.....	11
Figure 2- 5 Wind turbine generator with diode rectifier.....	12
Figure 2- 6 Wind turbine with diode rectifier and boost circuit	12
Figure 3- 1 Ideal power curve of a variable-speed wind turbine	15
Figure 3- 2 Variable-speed wind turbines with PMSG.....	16
Figure 3- 3 $C_p(\lambda)$ curve of the case study wind turbine	17
Figure 3- 4 Inverse Park transform	20
Figure 3- 5 Modelled $C_p(\lambda)$ curve	22
Figure 3- 6 Wind turbine generator power output vs rotor speed with different wind speed.....	22
Figure 3- 7 Inverse Clarke transform model.....	23
Figure 3- 8 From the rotor reference frame to the 3-phase symmetrical frame	23
Figure 3- 9 Simulation model of wind turbine generator.....	24
Figure 3- 10 The current output of the PMSG	25
Figure 4- 1 The topology of diode rectifier VSC.....	27
Figure 4- 2 The topology of back-to-back VSC.....	28
Figure 4- 3 The topology of step-down (Buck) converter	29
Figure 4- 4 Waveforms of a buck circuit in CCM	30
Figure 4- 5 The topology of step-up (boost) converter	31

Figure 4- 6 Waveforms of boost converter in CCM	32
Figure 4- 7 Rectifier with closed-loop boost chopper.....	34
Figure 4- 8 Simulation model of the AC to DC converter.....	34
Figure 4- 9 Boost PWM generator model	35
Figure 4- 10 Wind turbine output	36
Figure 4- 11 Current flow through the inductor.....	37
Figure 4- 12 3-phase AC voltage output from PMSG	37
Figure 4- 13 Rectifier bridge output voltage.....	37
Figure 4- 14 DC voltage output from the boost circuit.....	38
Figure 5 - 1 Framework of SVPWM algorithm	41
Figure 5 - 2 The topology of inverter.....	42
Figure 5 - 3 The patterns of voltage vectors	44
Figure 5 - 4 Cartesian to polar coordinates	46
Figure 5 - 5 The sinusoidal waves of three phase	46
Figure 5 - 6 Vector synthesis schematic in sector 1.....	48
Figure 5 - 7 The principle of PWM generator.....	50
Figure 5 - 8 The module of sector identified with Simulink	52
Figure 5 - 9 Simulation result of sector identified	52
Figure 5 - 10 The modelling of converting sector number in order.....	53
Figure 5 - 11 Result of converting sector number in order	53
Figure 5 - 12 Modelling of firing time of IGBTs.....	54
Figure 5 - 13 Firing time with over modulation.....	54
Figure 5 - 14 Modelling of generating carrier-wave in Simulink	55
Figure 5 - 15 The reference waveform with SVPWM.....	55
Figure 5 - 16 Modelling SVPWM.....	56
Figure 5 - 17 Output from inverter without filter.....	56

Figure 5 - 18 3-phase AC output from inverter.....	57
Figure 5 - 19 3-phase AC samples from power grid.....	57
Figure 6- 1 LVRT limit curve in German grid code	60
Figure 6- 2 LVRT curve from Nordel grid code.....	60
Figure 6- 3 LVRT curve from E.ON grid code.....	61
Figure 6- 4 The flowchart of filter algorithm.....	66
Figure 6- 5 Model of the voltage sag detection.....	67
Figure 6- 6 Only phase C with 20% drop	68
Figure 6-7 Both phase A and phase C with voltage sag	68
Figure 6- 8 Detection in the normal situation	69
Figure 6- 9 Nordel grid code	70
Figure 6- 10 German grid code	71

List of Tables

Table 5- 1 The relationship between work mode and phase voltage	42
Table 5- 2 The relationships between phase angle and phase's neutral voltage.....	47
Table 5- 3 The relationship of sector mapping	47
Table 6- 1 Comparison of conventional grid voltage detection techniques.....	63

List of Symbols

ρ	Air density, kg/m^3
λ	Tip speed ratio
A	Unit of current
C_p	Power coefficient
G	Gear ratio
I_{ds}	D-axis stator current, A
I_{qs}	Q-axis stator current, A
J	Moment of inertia, kgm^2
P	Number of poles
P_G	Wind turbine generator power output
P_t	Wind turbine rotor power
R	Wind turbine rotor radius
s	Slip
T_e	Electromagnetic torque, Nm
T_m	Input torque to the generator, Nm
T_t	Aerodynamic torque of wind turbine rotor, Nm
V	Unit of voltage, <i>Volt</i>
V_{ds}	Direct-axis stator terminal voltage, V
V_{qs}	Quadrature-axis stator terminal voltage, V
ω	Angular velocity of wind turbine rotor, <i>rad/sec</i>
ω_r	Angular velocity of generator rotor, <i>rad/sec</i>
ω_s	Synchronous speed in <i>rad/s</i>
$\frac{d}{dt}\psi_{ds}$	Amplitude of flux linkages, $v/rad/sec$
v	Wind speed, m/s

Chapter 1 Introduction

1.1 Background introduction

With the current rapid industrial development in the world, energy shortage has become one of the biggest issues many countries are facing. As a consequence of rising fossil fuel price and advanced technology, more and more homes and businesses have been installing small wind turbines for the purposes of cutting energy bills and carbon dioxide emissions, and are even selling extra electricity back to the national grid (BWEA 2009).

In small wind energy sector, UK has become the second largest market in the world. There are a large number of small wind turbines that have been installed in the UK between 2005 and 2008. By 2008, the total capacity of small wind turbine generation had reached 7.24 MW (BWEA 2009). The UK is not only a big market for wind small turbines, but also has many manufacturers of small wind turbines, with about 50% of world's small wind turbines made in the UK (BWEA 2009).

However, as wind is an intermittent renewable source, the wind source extracted by a wind turbine is therefore not constant. For this reason, the fluctuation of wind power results in fluctuated power output from wind turbine generator. From the point of view of utilities, due to the fluctuation of generator output, it's not appropriate for the generator to be directly connected to the power grid. In order to achieve the condition that the generator output power is suitable for grid-connection, it is necessary to use a controller to manage the output produced by the wind turbine generator.

The control technology relating to large wind turbines is sophisticated in terms of generator speed, and torque control, pitch angle control, maximum power point tracking (MPPT), and so on. However the control of small wind turbines still requires more concentrated efforts on the aspects of the wind turbine protection, over loading, and the maximum power output (Horizon Gitano-Briggs 2010).

This project will address the generator control of a small wind turbine for grid connection. The wind turbine extracts the energy from the wind through the rotor, which drives the generator to produce electricity.

There are various types of generators for wind turbines. Particularly, according to their electric energy produced, there are alternating current (AC) and direct current (DC) generators, where the AC generators are further classified as single-phase or poly-phase generators (Espinoza J.R. 2001; Kirtley J.L. 2010).

This project focuses on 3-phase AC Permanent Magnet Synchronous Generator (PMSG).

1.2 Aims and objectives

This project aims to model and simulate the controller of a grid-connected 3-phase PMSG, which will be fitted in a fixed-pitch variable-speed small wind turbine. In essence, the wind turbine will be used to provide electricity for a property, such as a farm, with mains electricity supply in the UK.

The whole simulation system consists of models of PMSG, AC/DC rectifier, DC/DC converter, DC/AC inverter, and grid voltage monitoring unit, which are detailed below. The objectives of the project are to develop the above mentioned mathematical and simulation models, and to verify the models through a case study simulation.

The system consists of the following major blocks:

- 1** AC/DC rectifier: The AC/DC rectifier is a full bridge circuit.
- 2** DC/DC converter: The boost circuit with close-loop control is employed to stabilise the voltage of DC bus at 400V for grid connection (Henryk Markiewicz and Antoni Klajn 2004). To allow the system controller to produce the described functionality, the control system takes the voltage information from the rectifier output and the chopper circuit generates a Pulse Width Modulation (PWM) signal to regulate the output voltage of the DC/DC converter.
- 3** DC/AC inverter: Space-Vector Pulse Width Modulation (SVPWM) is chosen to implement the DC/AC inverter. The System Controller takes the frequency, voltage and current signals from the power grid and its own output terminal, in order to generate a 6-channel PWM signal to control the Insulated Gate Bipolar Transistor (IGBT) blocks so as to achieve a closed loop full-bridge voltage source inverter (VSI). The model of the inverter will output a 50 Hz, 3-phase 400V AC (Henryk Markiewicz & Antoni Klajn 2004).
- 4** Monitor the power grid: This module is developed to detect the voltage sag of the power grid.

1.3 The framework of system

The case study wind turbine used for this project is the UCLan 10kW field testing research wind turbine. Appendix-A provides the details of the wind turbine and associated PMSG.

Figure 1-1 shows the control system framework which will be developed using MATLAB/Simulink. As Figure 1-1 illustrated, this project will concentrate on the modules of AC/DC, DC/DC and DC/AC converter. Apart from the converters, this

project will also address the detection of voltage sag from the power grid, which is essential for low voltage ride through for wind turbine generators.

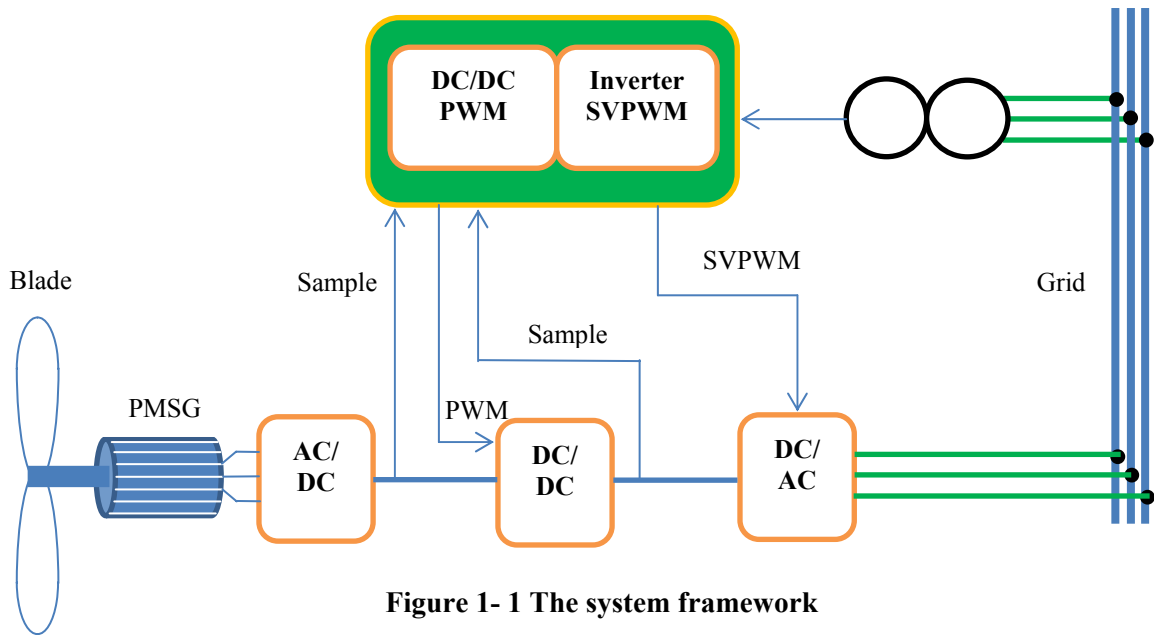


Figure 1- 1 The system framework

1.4 Structure of thesis

Chapter 2 provides a comprehensive overview in terms of the theory, technology and methodology, in which the primary focus is on PMSG wind turbine connection to the power grid.

Chapter 3 describes how wind turbines extract energy from wind. This chapter gives the mathematical model of PMSG, and discusses coordinate transformation from DQ orthogonal reference frame to 3-phase balance frame system.

Chapter 4: The chapter covers rectifier and DC to DC converter. In this chapter, the primary aims are to model the boost circuit in order to stabilise the voltage of DC bus for the purpose of providing DC power to the inverter. It makes a comparison between rectifiers based on diode and active switching devices. In the DC to DC part, the characteristics of bulk and boost chopper circuit are also introduced.

Chapter 5: The chapter describes the principle of the inverter in detail based on SVPWM, and elaborates the control of how to connect the inverter to the grid according to the feedback from the power grid.

Chapter 6: In this chapter, a novel method based on DQ transform is introduced to meet the detection of grid voltage sag, and a comparison is made with existing approaches.

The conclusion and future work are summarized in **Chapter 7**.

Chapter 2 Literature Review

2.1 Wind energy conversion system modelling

A wind turbine extracts kinetic energy from the wind to drive the wind turbine rotor, which is connected to a generator producing electricity (Johnson G.L. 2006). The maximum power output from the wind turbine is limited by the power coefficient C_p which is a function of the tip speed ratio λ . C_p never exceeds 59.3%, the Betz Limit (Hau Erich 2006). In general, C_p is between 25% - 45% (Anaya-Lara O., et al. 2009b).

The power (P_t) extracted from the wind by a wind turbine rotor can be expressed as:

$$P_t = \frac{1}{2} \rho C_p \pi R^2 v^3 \quad (2-1)$$

(Burton T., et al. 2001)

where

R is the wind turbine rotor radius

ρ is the air density

v is the wind speed

The tip speed ratio can be expressed as:

$$\lambda = \frac{R\omega}{v} \quad (2-2)$$

(Burton T., et al. 2001)

where ω is the angular velocity of the wind turbine rotor.

2.2 Wind turbine control for grid connection

In the book “Wind Energy Generation Modelling And Control”, the authors comprehensively classified wind turbine grid connection into three classes: direct-

coupled generator grid connection, doubly-fed induction generator grid connection and fully rated converter grid connection (Anaya-Lara O., et al. 2009b).

2.2.1 Direct-coupled generator grid connection

Fixed-speed squirrel-cage induction generators were widely employed for large wind turbine in 1980s, during which most of the technologies of wind turbines were direct-coupled generator grid connection, i.e. the wind turbine generator is directly coupled with the power grid. Due to the variation of the wind speed, the generator rotor speed is required to change slightly to balance the variation of the driving torque. The rotational speed of the generator is therefore not entirely constant. For a wound rotor induction generator, in order to produce magnetic field, it is necessary to provide extra power supply for the rotor circuit via a slip-ring. However the variation of the rotational speed is generally less than 1% due to the nature of small slip of induction generators (Anaya-Lara O., et al. 2009a), which is definition as the rate of the differential of the rotation speed of magnetic fields between the synchronous speed and rotation speed, divided by the synchronous speed(Shaw S.R. and Leeb S.B. 1999), it is describes in equation (2-1).

$$s = \frac{\omega_s - \omega_r}{\omega_s} \quad (2-1)$$

(Shaw S.R. & Leeb S.B. 1999)

where

s : slip

ω_s : synchronous speed in rad/s

ω_r : Angular velocity of generator rotor speed in rad/s

In general, the squirrel-cage induction generator needs to consume reactive power. For this reason, the generator normally requires compensation for reactive power by connecting it to a capacitor bank.

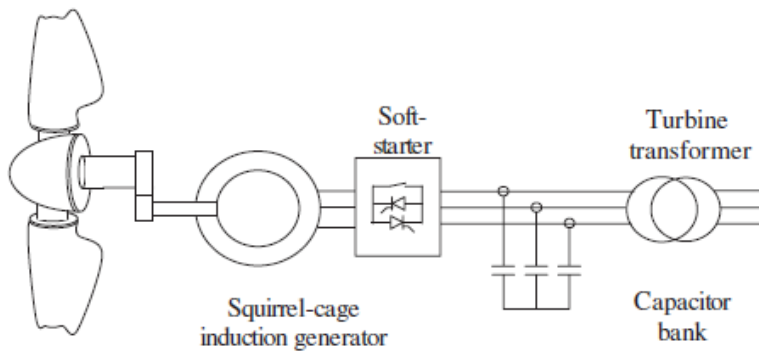


Figure 2- 1 Schematics of a fixed-speed wind turbine

Taken from (Anaya-Lara O., et al. 2009b)

Figure 2-1 illustrates a configuration of fixed-speed wind turbine, which consists of a squirrel-cage induction generator, bridge soft starter, a set of capacitor bank and a transformer. The advantages of this type of wind generation are:

- Simple structure
- Low cost
- Easy to maintain
- Simple solution for grid connection
- High performance-to-price ratio

However, there are a number of problems with fixed-speed wind power generation. First, the wind turbine does not operate under optimal tip speed ratio (or maximum power point tracking) with wind speed variation. This causes low efficiency of the wind turbine. Furthermore the squirrel-cage induction generator has low efficiency and power factor, and it requires an extra power supply (reactive power) for excitation (Hau Erich 2006).

2.2.2 Doubly-fed induction generator (DFIG) grid connection

The technology of doubly-fed induction generators is becoming more and more common due to the disadvantages of fixed speed induction generator. Variable speed DFIG is also an asynchronous generator, the common characteristics of doubly-fed and

fixed-speed generator is that their stator windings can directly be connected to the grid. Power output from the stator of a DFIG can be delivered directly to the grid, and the generator rotor absorbs excitation current from the grid. As Figure 2-2 illustrated, the rotor of DFIG connects to the grid by means of power converter. The power converter is able to transfer power bi-directly, which means it can deliver power to the grid and is also able to absorb power from the grid, depending on the rotational speed of the generator (Anaya-Lara O., et al. 2009b).

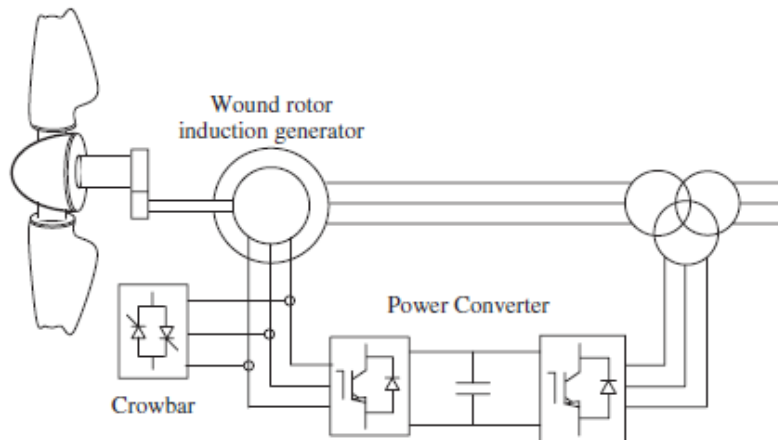


Figure 2- 2 The typical configuration of DFIG wind turbine

Taken from (Anaya-Lara O., et al. 2009b)

2.2.3 Fully rated converter grid connection

Figure 2-3 illustrates the characteristics of wind turbine configuration with fully rated converter grid connection. The wind turbine, with or without a gearbox, is fitted with either an induction generator or a permanent magnet synchronous generator (PMSG), and is connected to the grid with a fully rated power converter (Anaya-Lara O., et al. 2009b).

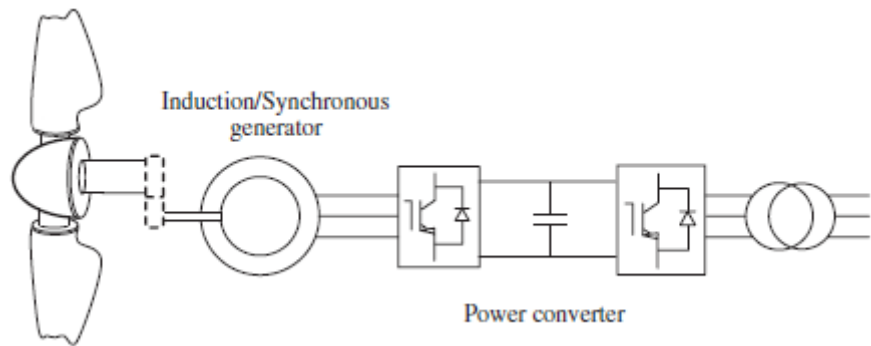


Figure 2- 3 Fully rated converter grid connection

Taken from (Anaya-Lara O., et al. 2009b)

The advantages of fully rated converter grid connection are:

- 1) The generator is completely decoupled from the grid, which means the power factor can be corrected by an active filter, i.e. the inverter can improve the output power quality with an unit power factor before injection to the power grid.
- 2) It allows variable-speed operation of the wind turbine, which enables maximum power point tracking (MPPT) between cut-in wind speed and rated wind speed.

In this project the PMSG is chosen for the wind turbine generator, and the power output from the generator is fully rated delivered to the grid through a power converter. The frequency and voltage of the power output from a PMSG varies with the rotational speed of the generator.

For this project, the configuration of the PMSG fully rated converter grid connection consists of AC/DC rectifier, DC/DC converter and DC/AC inverter.

2.2.4 AC/DC Rectifier and DC/ DC converter

There are a number of papers which discussed the strategy of grid connection for PMSG wind turbines. The most popular control topology is the back-to-back converter as Figure 2-4 shows.

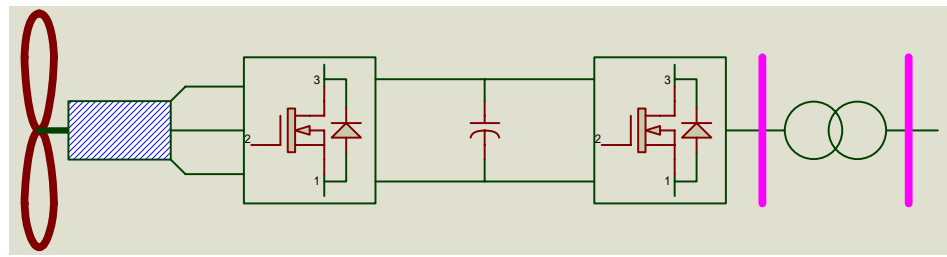


Figure 2- 4 Wind turbine PMSG with back-to-back converter

Taken from (Busca C., et al. 2010)

The characteristics of the back-to-back converter are that the converter utilises active devices at both the generator side for the rectifier and the grid side for the inverter (Bharanikumar R., et al. 2010).

The advantages of back to back converter are as follows:

- The rectifier is controllable, and
- Both rectifier and inverter bridges are composed of active IGBT devices, with the current be able to flow from either the generator to the grid or the grid to the generator.

The major disadvantage of back-to-back topology is:

- The controller is complex and expensive because it requires 12-channel Pulse Width Modulation (PWM) signals for the rectifier and the inverter. For this reason, in a practical application, the control system requires at least two or more Micro-Controller Units (MCU), Digital Signal Processor (DSP), Field Programmable Gate Array (FPGA), etc. to control the chips on the board.

A simple topology for wind turbine generation was introduced by Tarek Ahmed (Ahmed T., et al. 2004) and is illustrated in Figure 2-5, which consists of a diode bridge rectifier, with a DC link to an active IGBT inverter.

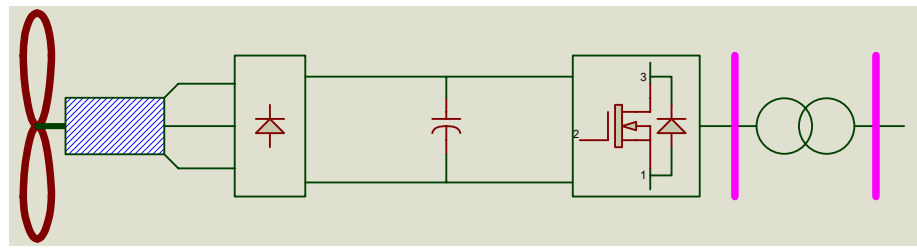


Figure 2- 5 Wind turbine generator with diode rectifier

Taken from (Wang Quincy and Chang Liuchen 2004)

Although this type of converter is simple and reliable, but the power factor of the generator is low. The other problem is that when the output voltage of the rectifier is lower than the grid, power cannot be injected to the grid.

By summarising the topology of back-to-back and diode rectifier, it is possible to insert a boost circuit between the diode rectifier and the inverter, in order to solve the issue of generator power factor, as shown in Figure 2-6. There have been a number of papers describing the inclusion of Power Factor Correction (PFC) with boost circuits, however only a few papers discuss it with the wind turbine controller (Belakehal S., et al. 2009; Bana Sharifian M.B, et al. 2009).

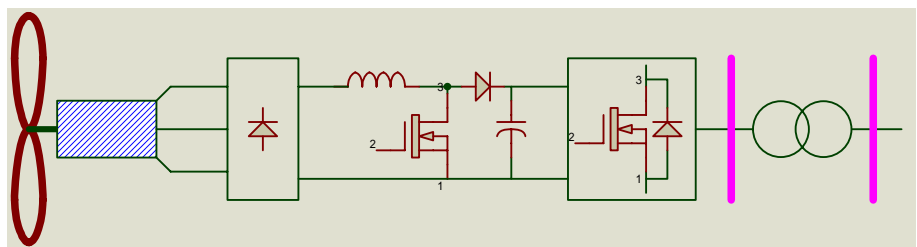


Figure 2- 6 Wind turbine with diode rectifier and boost circuit

For this topology of converter, operation at relatively low wind speeds is possible due to the inclusion of the boost circuit. The boost circuit can maintain the DC bus link voltage at a constant value. This topology is utilised for the converter in this project.

2.2.5 Inverters for grid connection

Currently, the most popular technology of Direct Torque Control (DTC) for electrical motor, was first introduced by Depenbrock and Takashia (Meziane R.T.S. and Benalla H. 2007). Depenbrock first presented the concept of DTC based on regular hexagon flux control in 1988 (Depenbrock M. 1988). In this paper, the flux was controlled in accordance to the hexagon running, and the six sides of hexagon correspond with six vectors of voltage (Quang N.P. and Dittrich J.A. 2008). Therefore it is simple to achieve flux control by means of three Schmitt triggers (Depenbrock M. 1988). The characteristics of this control strategy are of simple, low switching times, and low loss. For this reason, the strategy is appropriate for application where switching frequency is low with large power. However, the output voltage and current waveforms include serious distortion.

Another popular control strategy of DTC is presented by I. Takashashi in 1986 (Takahashi Isao and Noguchi Toshihiko 1986). The control flux of motor approximately runs against a circular track. By means of a control system, the error between the torque of motor and the flux is estimated in real-time and referred to the spatial position of the flux of the stator to choose the corresponding switching vectors. This forces the track of flux to gradually approach a circular shape. Because the flux track approximately approaches a circle, this results in significant reduction in the harmonic. The control system is relatively complicated, and high switching frequency and large electrical surges are produced. With the development of modern power electronic devices, these devices can drive large load with high switching frequency. This control strategy is suitable for PMSG system, and is employed in the inverter of this project.

2.3 Summary

The literature review detailed in this chapter has led to a comprehensive understanding of the concepts relevant to the control of permanent magnet synchronous generators for wind turbines with grid-connection.

Chapter 3 PMSG Modelling for Variable-Speed Wind Turbine

3.1 Introduction to variable-speed wind turbine with PMSG

Variable-speed wind turbine has the advantage to follow the variation of wind speed and produce the maximum power under the normal operation at low wind speed (below rated wind speed) through maximum power point tracking (MPPT). When the wind speed is higher than rated wind speed, the wind turbine generally works under constant power output through either generator load control or pitch control or both if possible. Figure 3-1 displays the ideal power curve of the case study wind turbine, which is variable-speed wind turbine. In the Figure 3-1 Region II shows that the turbine output follows the MPPT curve.

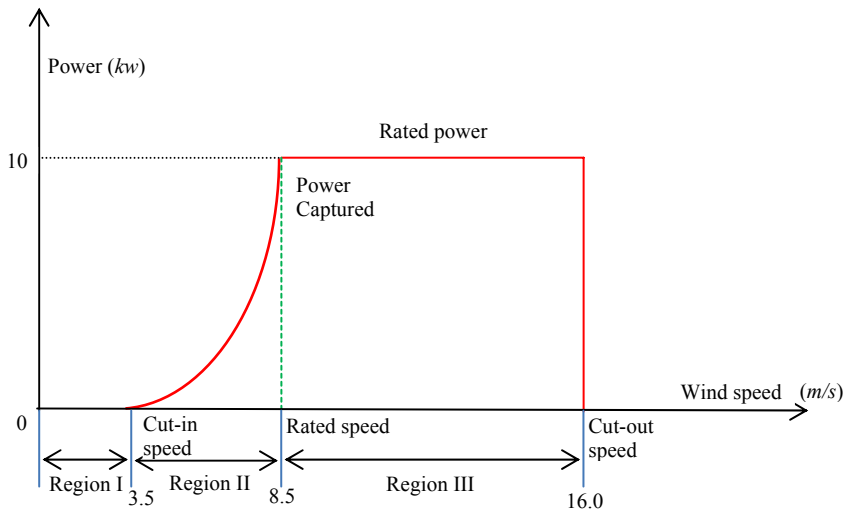


Figure 3- 1 Ideal power curve of a variable-speed wind turbine

Variable-speed wind turbine can use both synchronous generator and doubly-fed induction generator. The synchronous generator can either be permanent magnet synchronous generator (PMSG) or excited magnet synchronous generator. The excited magnet synchronous generator requires an extra DC power supply to the rotor windings to produce a rotating magnetic field. The magnetic field can be controlled by regulating the

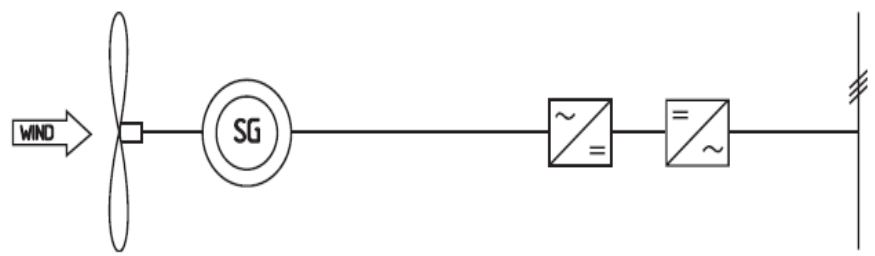
flow current of the rotor windings. The generator output varies with the rotor speed and the exciting DC current. In contrast, the magnetic field of a PMSG cannot be controlled.

Small wind turbines are favoured with PMSG due to the following advantages:

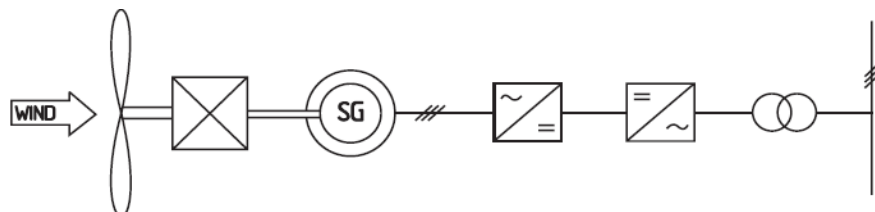
- The system is simple and reliable
- It has less transmission losses
- It has high efficiency of generator
- The generator is without excitation and brushless
- It has high quality output and does not need to compensate for reactive power

This thesis will address the control of variable-speed wind turbine with PMSG.

There are two common topologies for variable-speed wind turbines with PMSG: i.e. direct-driven (without a gearbox) and hybrid transmission (with one stage planetary gear), as illustrated in Figure 3-2. The case wind turbine used for this project is a direct-driven variable-speed wind turbine with PMSG, however the control modules proposed in the thesis are also suitable for hybrid transmission variable-speed wind turbines with PMSG.



(a) Direct driven



(b) Hybrid transmission

Figure 3- 2 Variable-speed wind turbines with PMSG

Taken from (Anaya-Lara O., et al. 2009b)

Both the frequency and amplitude of the voltage output from a variable-speed PMSG vary due to the changing wind speed; therefore the need for full power conversion for grid connection, i.e. AC/DC and DC/AC conversion, as illustrated in Figure 3-2.

3.2 Wind turbine aerodynamic characteristics

As stated in Chapter 2, the power from a wind turbine rotor can be expressed as (Johnson G.L. 2006):

$$P_t = \frac{1}{2} C_p(\lambda) \rho \pi R^2 v^3 \quad (3-1)$$

where $C_p(\lambda)$ is the non-dimensional power coefficient, which represents the aerodynamic performance characteristics of the wind turbine rotor. The power coefficient C_p is a function of the wind turbine blade tip speed ratio λ , which is given by (Borowy Bogdan S. and Salameh Ziyad M. 1997):

$$\lambda = \frac{R\omega}{v} \quad (3-2)$$

The $C_p(\lambda)$ curve is turbine specific and depends particularly on its blade design. Figure 3-3 shows the $C_p(\lambda)$ curve of the case study wind turbine of this project, i.e. the 10kW field testing research wind turbine with a direct-driven PMSG, as detailed in Appendix-A. The top value of the C_p is 0.43 when the tip speed ratio $\lambda=8$.

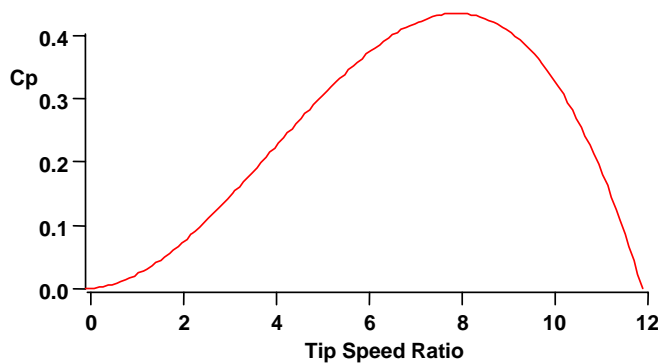


Figure 3- 3 $C_p(\lambda)$ curve of the case study wind turbine

(Taken from PhD student Xin Zhi Tang)

The aerodynamic torque of a wind turbine rotor can be expressed as follows (Johnson C.C. and Smith Richard T. 1976):

$$T_t = \frac{P_t}{\omega} = \frac{1}{2} \frac{C_p(\lambda)}{\lambda} \rho \pi R^2 v^2 \quad (3-3)$$

The wind turbine generator power output can be expressed as follows

$$P_G = \frac{1}{2} \eta C_p(\lambda) \rho \pi R^2 v^3 \quad (3-4)$$

where η is the total efficiency of the mechanical transmission system and the generator.

For the case study of the 10kW wind turbine, when it operates at rated speed 130rpm at rated wind speed 8.5m/s, the total efficiency of the wind turbine system is $\eta = 78.72\%$.

3.3 Mathematical modelling of PMSG

In order to develop the mathematical model for a PMSG, it is essential to make the following assumptions (Arroyo E.L.C. 2006):

- The conductivity of the permanent magnet is zero
- Saturation is neglected
- Induced electromotive force (EMF) is sinusoidal
- Eddy currents and hysteresis losses are negligible
- There are no field current dynamics

With the assumptions above, the wind turbine causes the rotor of the PMSG to rotate. This can be represented in the direct-quadrature (DQ) coordinate system, which is described as follows (Borowy Bogdan S. & Salameh Ziyad M. 1997):

$$V_{qs} = -r_s i_{qs} + L_{qs} \frac{d}{dt} i_{qs} - \omega_r L_{ds} i_{ds} + \omega_r \frac{dy}{dx} \psi_{ds} \quad (3-5)$$

$$V_{ds} = -r_s i_{ds} + L_{ds} \frac{d}{dt} i_{ds} + \omega_r L_{qs} i_{qs} \quad (3-6)$$

where

V_{qs} is the quadrature-axis (q-axis) stator terminal voltage in volt

V_{ds} is the direct-axis (d-axis) stator terminal voltage in volt

i_{ds} is the d-axis stator current in ampere A

i_{qs} is the q-axis stator current in ampere A

ω_r is the angular velocity of generator rotor in rad/sec

r_s is the equivalent resistance of the stator winding

L_{ds} is the stator equivalent inductance in d-axis

L_{qs} is the stator equivalent inductance in q-axis

$\frac{d}{dt} \psi_{ds}$ is the amplitude of the flux linkages in v/rad/sec

In the rotor reference frame, the electromagnetic torque can be described by:

$$T_e = \frac{3P}{4} \left[i_{ds} i_{qs} (L_{ds} - L_{qs}) + i_{qs} \frac{d}{dt} \psi_{ds} \right] \quad (3-7)$$

where T_e is electromagnetic torque in Nm

P is the pole number of generator stator

The relationship between the angular velocity of the generator rotor and the mechanical angular velocity of the wind turbine rotor is given as follows (Bharanikumar R., et al. 2010):

$$\omega = \frac{2\omega_r}{PG} \quad (3-8)$$

$$\frac{d}{dt} \omega_r = \frac{P}{2J} (T_m - T_e) \quad (3-9)$$

where

G is the gear ratio

T_m is the input torque to the generator rotor in Nm

J is the inertia of the generator rotor in kgm^2

The input torque to the generator can be obtained by means of the torque of wind turbine rotor divided by the gear ratio.

$$T_m = \frac{T_t}{G} \quad (3-10)$$

Here it is assumed that the torque loss through the mechanical transmission system is neglected. For a direct-driven PMSG wind turbine, $G=1$, and $T_m = T_t$.

3.4 Mathematical inverse Park and Clarke transforms

The discussion above is based on the rotating reference frame. A practical generator produces 3-phase AC power. For this reason, the inverse Park and Clarke transforms are introduced to implement the 3-phase AC output from the generator model.

As Figure 3-4 shows, the transform from the stator axis reference frame ($\alpha\beta$) to the rotating reference frame (dq) is called the Park transform (Texas Instruments 1997). The Clarke transform is the transformation of the 3-phase reference frame to the 2-phase orthogonal stator axis ($\alpha\beta$).

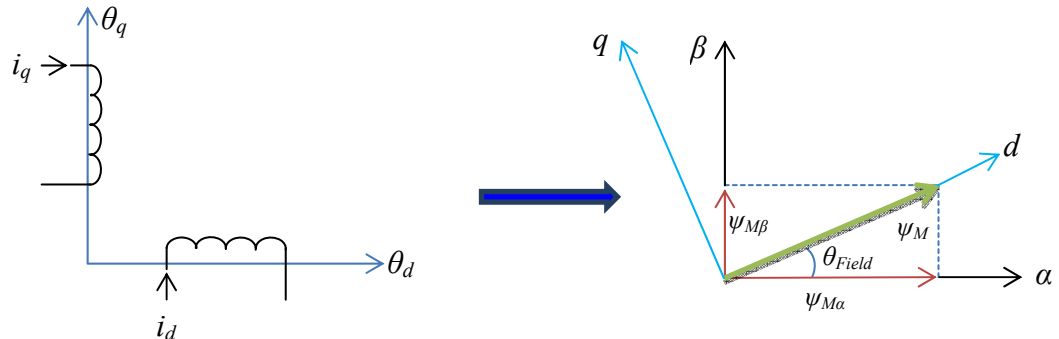


Figure 3- 4 Inverse Park transform

As Figure 3-4 illustration, assumes the $\alpha\beta$ frame has an angle θ_{Field} with the dq frame, the inverse Park transform ($dq - \alpha\beta$) which can be expressed as follows:

$$\begin{bmatrix} \alpha \\ \beta \end{bmatrix} = \begin{bmatrix} \cos \theta_{Field} & -\sin \theta_{Field} \\ \sin \theta_{Field} & \cos \theta_{Field} \end{bmatrix} \begin{bmatrix} d \\ q \end{bmatrix} \quad (3-11)$$

The mathematical inverse Clarke transform is given as follows:

$$\begin{bmatrix} V_a \\ V_b \\ V_c \end{bmatrix} = \begin{bmatrix} 1 & 0 \\ -\frac{1}{2} & \frac{\sqrt{3}}{2} \\ -\frac{1}{2} & -\frac{\sqrt{3}}{2} \end{bmatrix} \begin{bmatrix} \alpha \\ \beta \end{bmatrix} \quad (3-12)$$

3.5 Modelling PMSG with MATLAB/Simulink

In order to simulate the power generation from the wind turbine, it is necessary to model the wind and obtains the power coefficient of the wind turbine rotor using MATLAB.

3.5.1 Simulation of wind turbine rotor power coefficient

There are many of mathematical models which can be used to describe the relationship between the power coefficient and the tip speed ratio. However most of them are based on variable-pitch wind turbine. The case study 10kW wind turbine is a fixed-pitch wind turbine, the $C_p(\lambda)$ curve of the wind turbine can be expressed approximately using the following polynomial (Borowy Bogdan S. & Salameh Ziyad M. 1997):

$$C_p(\lambda) = a_1 + a_2\lambda + a_3\lambda^2 + a_4\lambda^3 + a_5\lambda^4 + a_6\lambda^5 \quad (3-13)$$

Through adjusting the coefficients $a_1 \sim a_6$ in the above polynomial equation (3-13), the shape of the $C_p(\lambda)$ curve can be modified. Programming a MATLAB code (Appendix - B), after repeatedly adjusting the polynomial coefficients $a_1 \sim a_6$ based on the specification of the case study wind turbine (Appendix - A), an appropriate set of coefficients $a_1 \sim a_6$ are confirmed as the following equation.

$$C_p(\lambda) = 0.052 - 0.118\lambda + 0.16\lambda^2 - 0.062\lambda^3 + 0.0102\lambda^4 - 0.000565\lambda^5 \quad (3-14)$$

Figure 3-5 depicts the calculated $C_p(\lambda)$ curve of the case study 10kW wind turbine based on Equation (3-14).

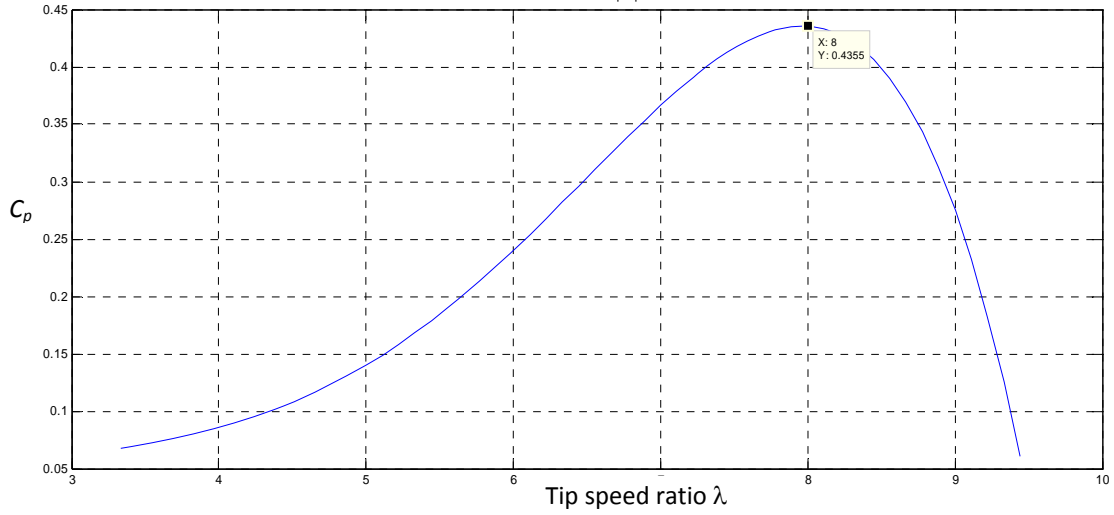


Figure 3-5 Modelled $C_p(\lambda)$ curve

Figure 3-5 shows that the top value of the rotor aerodynamic power coefficient C_p at the rated wind speed is 0.4355, and the corresponding tip speed ratio is 8. The $C_p(\lambda)$ curve is approximately the same as illustrated in Figure 3-3.

3.5.2 Simulation of wind turbine generator power output

Based on Equation (3-4) and (3-13), the relationship between the generator power output and the rotor speed of the case study 10kW wind turbine with different wind speed can be drawn. This is shown in Figure 3-6, in which “v” denotes the wind speed.

The red dash line is the curve of maximum power point tracking (MPPT).

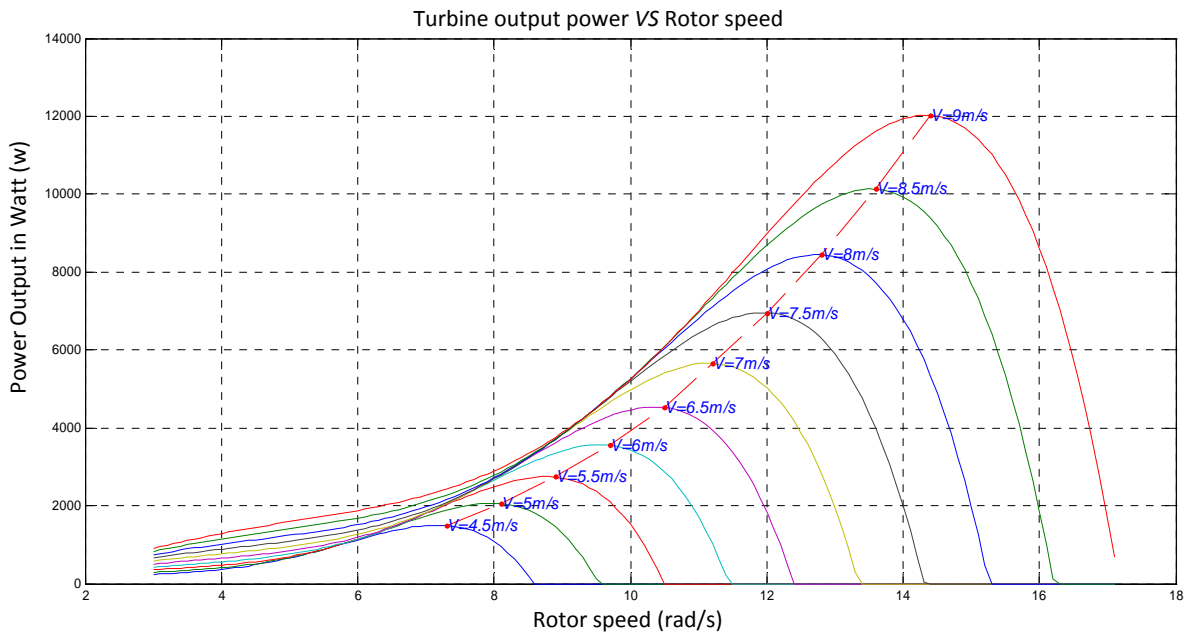


Figure 3-6 Wind turbine generator power output vs rotor speed with different wind speed

As shown in the figure, the generator power output is approximately 10.13kW when the turbine operates at rated wind speed 8.5m/s. The rotor speed of the wind turbine is 13.6rad/s, which is equivalent to 130rpm. The results meet with the specification of the case study 10kW wind turbine as detailed in Appendix-A.

3.5.3 PMSG Simulation

Figure 3-7 is the simulation model of the inverse Clarke transform of the case study PMSG. The model is developed with MATLAB/Simulink based on Equation (3-12). In the model, Alpha represents α and Beta denotes β in the static $\alpha\beta$ frame.

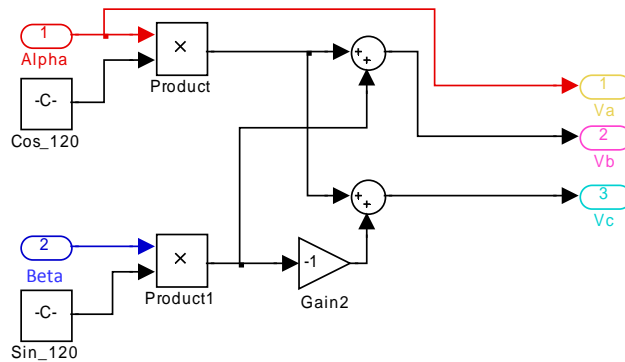


Figure 3- 7 Inverse Clarke transform model

Figure 3-8 shows that the model implements a series of transforms from the DQ coordinate system to the 3-phase balance frame. As the figure illustrates, the simulation model consists of two parts, i.e. the inverse Park and inverse Clarke transforms.

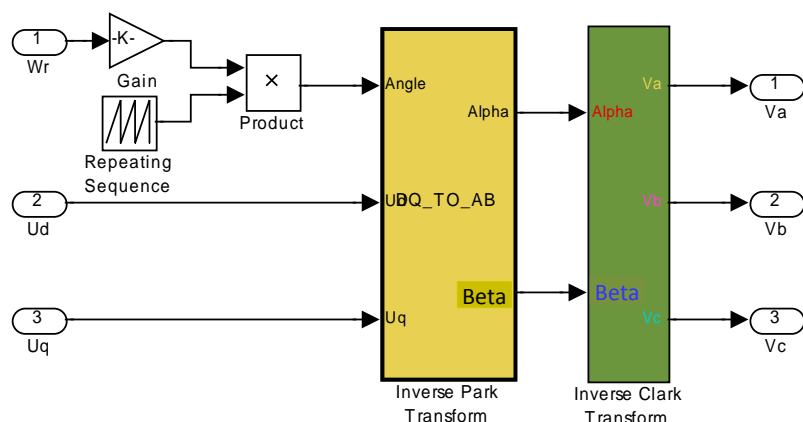


Figure 3- 8 From the rotor reference frame to the 3-phase symmetrical frame

The inverse Park transform function block in Figure 3-8 is used to implement Equation (3-11) and (3-12), and the MATLAB program of this block is listed below:

```
function [Alpha,Beta] = DQ_TO_AB(Angle,Ud,Uq)
Cos=cos(Angle);
Sin=sin(Angle);
Beta=Ud*Cos-Uq*Sin;
Alpha=Ud*Sin+Uq*Cos;
Beta=Beta/(sqrt(3))/400;
Alpha=Alpha/(sqrt(3))/400;
```

In order to obtain the current waveform of the generator power output, at the end of the code above, both of the two return parameters are divided by the power grid phase to phase voltage, i.e. 400V.

Figure 3-9 illustrates the complete simulation model of the wind turbine generator created with MATLAB/Simulink, under the condition of rated wind speed and rated rotational speed as Appendix-A lists.

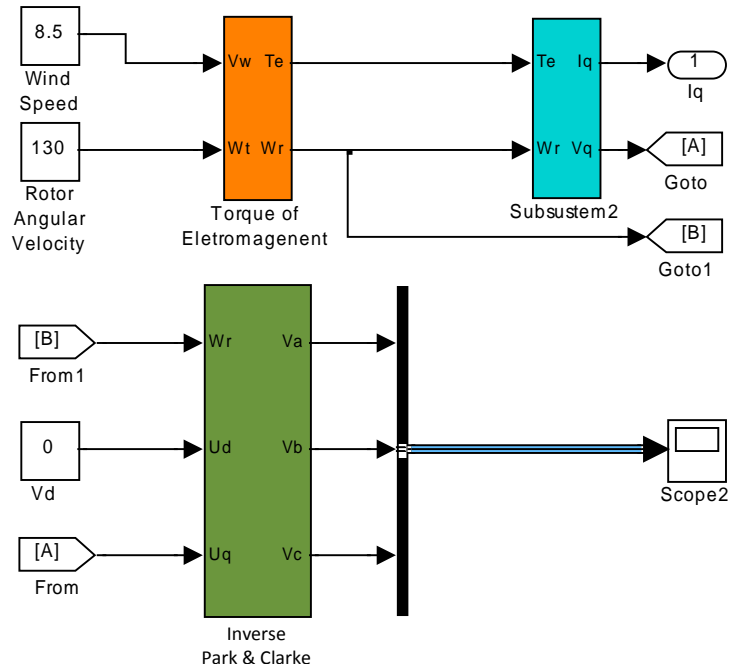


Figure 3- 9 Simulation model of wind turbine generator

Figure 3-10 shows the current output of the case study wind turbine generator, which operates at the rated wind speed 8.5m/s and rated rotor speed 130rpm. The specifications of the case study 10kW wind turbine generator are listed in Appendix-A.

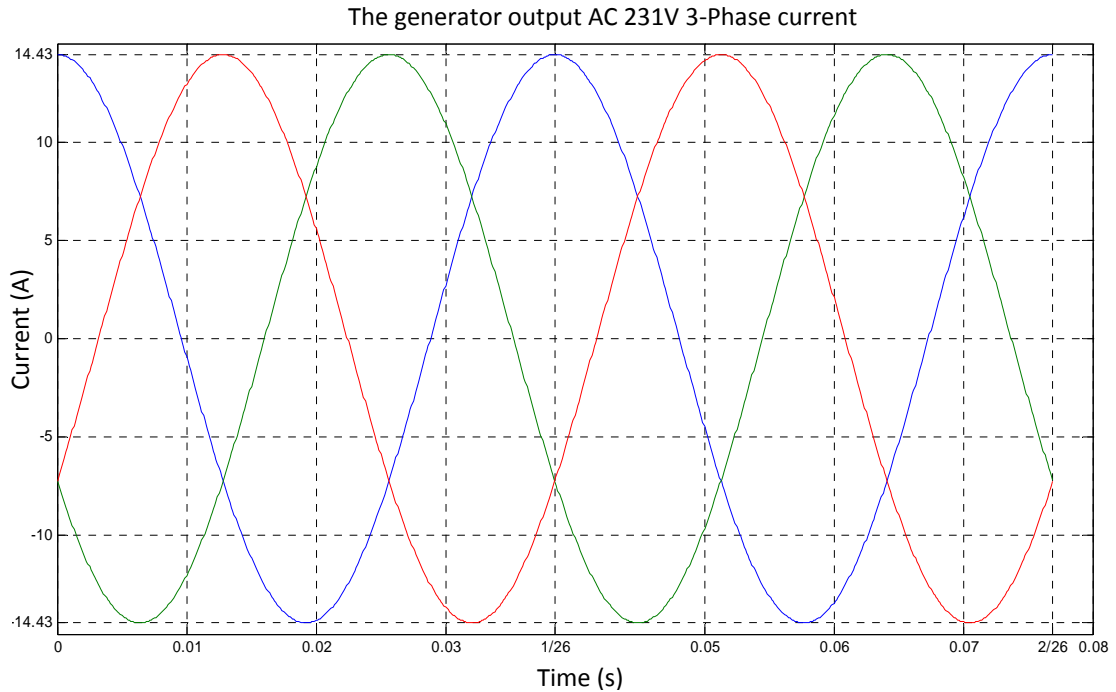


Figure 3- 10 The current output of the PMSG

The simulation shows that the current of the generator output is 14.43A and the frequency is 26Hz, which met the specifications of the case study wind turbine generator design: 10kW 3-phase AC (14.43A, 231V) power output.

3.6 Summary

This Chapter summarises the aerodynamic power performance of direct-driven, fixed-pitch, variable-speed wind turbines with PMSG, and presents the mathematical model of the case study 10kW PMSG for UCLan field testing research wind turbine. The transform from DQ orthogonal reference frame to 3-phase balance frame system is analysed and modelled.

The simulation outcomes demonstrate that the mathematical model of the wind turbine generator developed with MATLAB/Simulink is correct.

Chapter 4 AC/DC Rectifier and DC/DC Boost Circuits

4.1 Introduction

The wind resource is intermittent, which results in the unstable PMSG output. However, in order for the system to reliably connect to the power grid through the inverter circuit, the DC bus link is required to be stable at 415 V. Based on these requirements, the AC/DC rectifier and DC/DC boost circuits are employed in this project and this chapter discusses the AC/DC rectifier and DC/DC boost circuits.

4.2 Introduction of rectifier circuit

The amplitude and frequency of the voltage output from a PMSG vary for a variable speed wind turbine when the wind speed changes from time to time, while in this circumstance the generator power output should be stabilised.

The AC/DC converter circuits can be classified as uncontrolled rectifier and controlled rectifier circuits. In general, an uncontrolled rectifier circuit is made of some passive elements, such as resistors, diodes, capacitors, and etc. A controlled rectifier circuit generally employs some active elements, such as thyristors, Metal-Oxide-Semiconductor Field-Effect Transistors (MOSFET) or IGBTs to regulate its output voltage (Czarkowski D. 2001).

The most two common typical rectifier topologies employed in variable-speed PMSG wind turbine are:

- Diode bridge voltage source converters (VSCs)
- Back-to-back VSCs

4.2.1 Diode rectifier bridge VSCs

Figure 4-1 illustrates the topology of a typical power converter of PMSG for grid connection with a 3-phase diode bridge VSC. At the generator side, the rectifier circuit consists of 6 passive diodes, and at the grid side, the full bridge inverter is composed of 6 IGBTs. For this type of converter, the current from the wind turbine generator can only flow toward to the grid, i.e. one way power flows from the generator to the grid. AC power from the generator is converted into DC power through the rectifier diode bridge, and then inverted to AC for grid connection by means of the full IGBT inverter bridge.

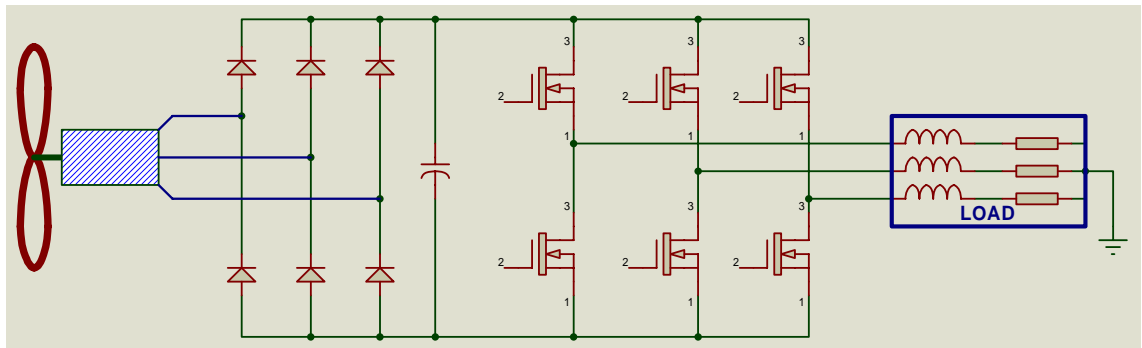


Figure 4- 1 The topology of diode rectifier VSC

This configuration decouples the wind turbine generator from the grid by the diode bridge. The VSC controller stabilises the voltage of the DC link using the capacitor between the rectifier diode-based bridge and the full IGBT inverter bridge.

Because most wind turbines work at start up with a large drag, especially for a large scale wind turbine, the wind turbine generator requires high torque to drive it. The popular solution for this problem is either to design a wind turbine with low start up wind speed or to provide an additional driver component.

Because the configuration of a back-to-back converter is bi-directional the generator can operate as a motor. In the situation of low wind speed, a back-to-back converter can

draw power from the grid to drive the motor (the generator) to provide the start-up torque.

Therefore, the primary disadvantage of the configuration based on diode rectifier is that it cannot draw power from the grid to drive the generator as a motor when it needs to start at very low wind speed.

4.2.2 Back-to-back VSCs

Figure 4-2 shows the rectifier circuit consisting of 6 active switching devices in the topology of a back-to-back VSC. This arrangement is bi-directional, and both circuits at the generator side and inverter side are symmetrical. At the generator side, in order to stabilise the DC bus voltage, the controller samples the voltage of the DC bus link and generator output, and locks the frequency output from generator to produce firing angle time for each of the switching devices after some calculations. At the inverter side, based on the voltage, frequency and amplitude of the power grid, the controller produces PWM signals to control the IGBTs conduction (Li S.H., et al. 2012; Zhou M.X., et al. 2011).

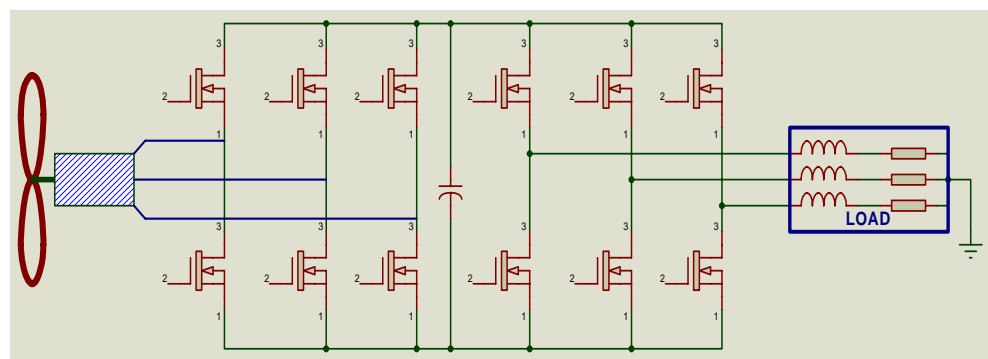


Figure 4- 2 The topology of back-to-back VSC

4.3 DC to DC converter

With the development of electronic technology, the quality of the power supply of DC/DC converters has improved considerably in terms of reliability, stability and efficiency.

The most widely used topologies of DC/DC converters are: Step-down (Buck) circuit, Step-up (Boost) circuit, Buck-Boost converter, etc.

Whatever topology of a DC/DC converter, according to the current flowing through the inductor L , the circuit operation is divided into 2 working modes. If the current through the inductor L is always positive and never equal to zero in any switching period in the switching device M , this is called the Continuous Conduction Mode (CCM) (Czarkowski D. 2001). Otherwise the operating mode is called the Discontinuous Conduction Mode (DCM) (Czarkowski D. 2001).

4.3.1 Step-down (Buck) converter

A step-down circuit is also known as a buck circuit as shown in Figure 4-3. The circuit consists of a voltage source V_s ; a switching device M , which is connected in series with the voltage source via Terminal 3; a diode D , which is reverse biased connected the switching device M to the ground via Terminal 1; a filter inductor L , which is in series with the combination of a filter capacitor C and a resistor load in parallel.

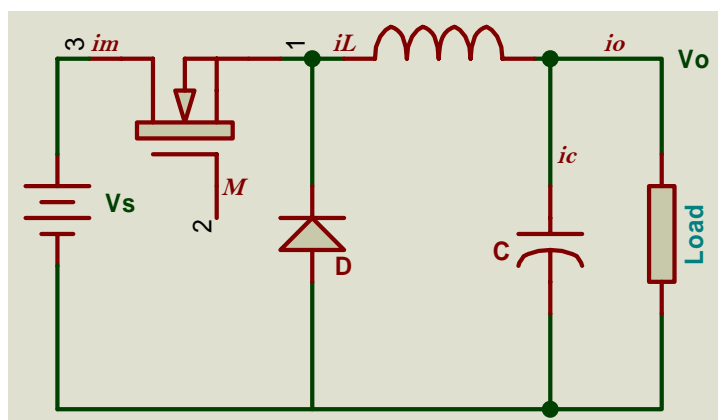


Figure 4- 3 The topology of step-down (Buck) converter

Figure 4-4 shows the relationship between the switching signal M , which is the input signal to the switching device M in Figure 4-3 via Terminal 2, the voltage source v_s , the output voltage of the circuit v_o , the buck current i_m , the inductor current i_L , the capacitor current i_C , the duty ratio D and the switching period T .

For a buck converter, from Figure 4-3 and Figure 4-4, the relationship between the input voltage, output voltage and the duty ratio of switching time D is obtained (Czarkowski D. 2001):

$$(V_s - V_o)DT = V_o(1 - D)T \quad (4-1)$$

Reorganising the equation above, we have the relationship A between the output voltage and input voltage of the buck circuit:

$$A \equiv \frac{V_o}{V_s} = D \quad (4-2)$$

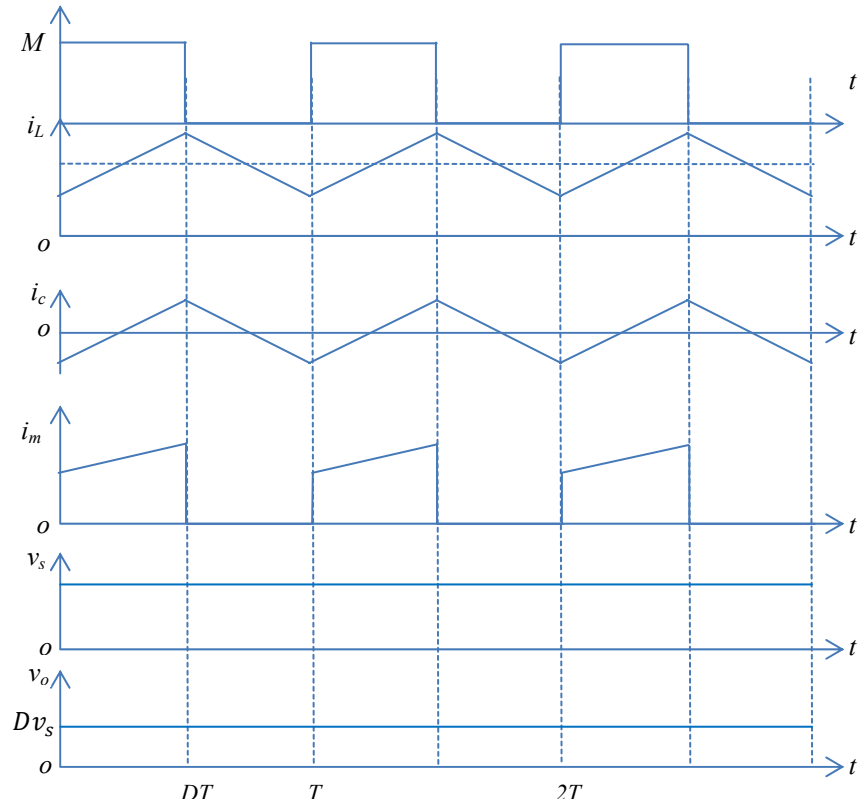


Figure 4- 4 Waveforms of a buck circuit in CCM

For the buck circuit, based on the Equation 4-2, it can be concluded that the input voltage is always greater than the output voltage.

If the switching frequency is fixed, the inductance L in the buck circuit determines the operating mode of the circuit, i.e. CCM or DCM. The critical inductance between CCM and DCM is given by (Czarkowski D. 2001):

$$L_c = \frac{(1-D^2)R}{2f} \quad (4-3)$$

4.3.2 Step-up (Boost) converter

Figure 4-5 illustrates a boost converter, which consists of a voltage source V_s , an inductor L , which is used for energy storage and connected to the voltage source in series, a switching device M , a diode D , a filter capacitor C and a load.

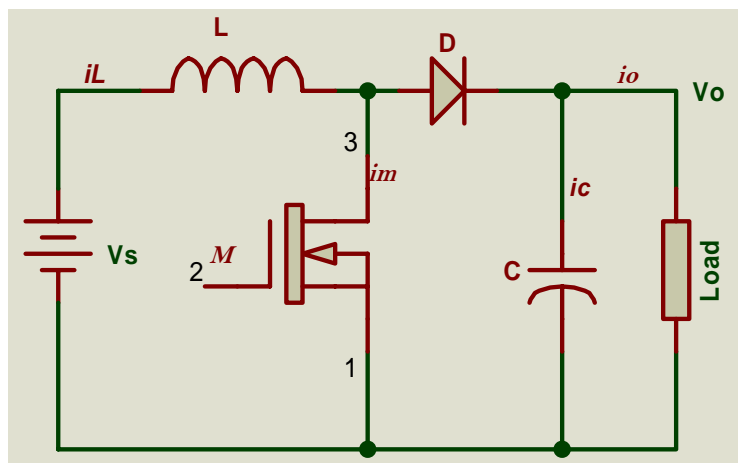


Figure 4- 5 The topology of step-up (boost) converter

Figure 4-6 illustrates that energy from the voltage source is stored in the inductor L when the switching device M is conducting. The current through the inductor increases linearly, the diode D is reverse biased and the capacitor provides voltage for the load during that time. When the switching device M is opened, the diode D conducting the current through the inductor L , and diode D offers power for the load and the charging of the capacitor C .

Using the Faraday's law, the relationship among the duty ratio D of the switching period for the IGBT M , the output voltage and the input voltage can be obtained as (Czarkowski D. 2001):

$$V_s DT = (V_o - V_s)(1 - D)T \quad (4-4)$$

Minimising the equation above gives

$$A \equiv \frac{V_o}{V_s} = \frac{1}{1-D} \quad (4-5)$$

where A is the gain of boost circuit.

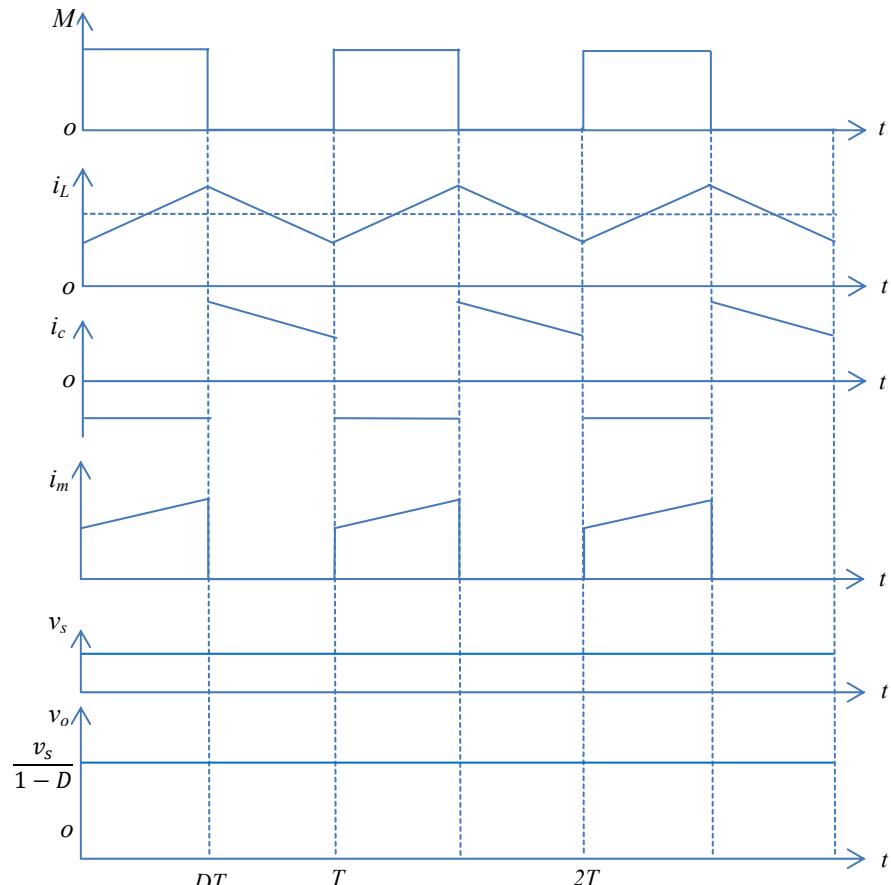


Figure 4-6 Waveforms of boost converter in CCM

Equation 4-5 shows that the gain of the boost circuit is always greater than 1, which means that the output voltage of the boost circuit is always higher than the input voltage.

The boost converter has the same characteristic as the buck converter. Once the switching frequency is confirmed, the inductance of L determines the operating mode of the circuit, as given by (Czarkowski D. 2001):

$$L_c = \frac{(1-D)^2 DR}{2f} \quad (4-6)$$

where L_c is the critical value of the inductance, D is duty ratio of the switching period, R is the resistance of the load and f is the switching frequency.

If the inductance L in the boost converter is greater than L_c , the converter operates in the state of CCM, otherwise it operates in the state of DCM.

4.4 Design of rectifier with closed-loop boost chopper

The primary characteristic of a boost chopper circuit is to increase the voltage. If the converter configuration consists of diode rectifier bridge and boost chopper circuit, it can reduce the cut-in wind speed for a wind turbine. This allows a low voltage output from the diode rectifier at a low wind speed. The boost circuit also can provide a stable DC voltage for the following inverter circuit. Because the current only flows from the generator to the grid, this configuration is appropriate for the occasions when the wind turbine can start its operation by itself with low wind speed 3 m/s.

Figure 4-7 illustrates a simple topology of a diode rectifier VSC for a wind turbine PMSG with grid-connection. The strategy inserts a boost circuit between the rectifier and inverter bridge, and adds a feedback circuit to maintain the DC output voltage. The feedback circuit compares the voltage from the filter capacitor and the reference voltage. The output from the differential amplifier is compared with a triangular wave to produce the PWM signal that will control the switching IGBT, and determines the duty ratio of the PWM signal. The PWM signal frequency is equal to the triangular wave's frequency.

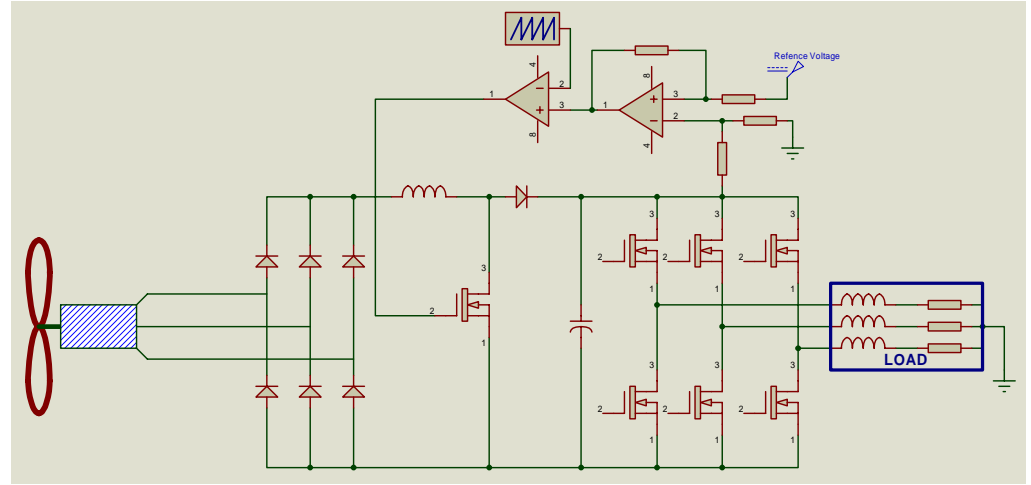


Figure 4- 7 Rectifier with closed-loop boost chopper

4.5 Modelling the rectifier with closed-loop boost chopper using MATLAB/Simulink

Figure 4-8 is the AC/DC converter simulation model developed with MATLAB/Simulink. In the simulation model, the PWM generator module takes the sampling voltage from the output of the boost circuit, the sampling voltage from the diode rectifier bridge output, and estimated current outputs from the PMSG based on MPPT, to regulate the duty ratio of the PWM.

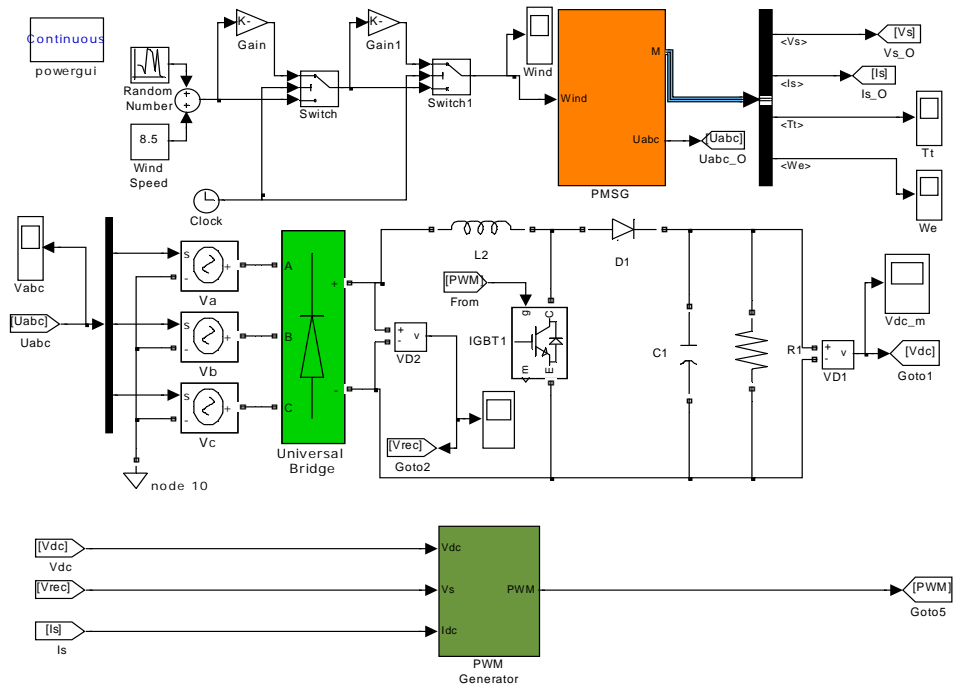


Figure 4- 8 Simulation model of the AC to DC converter

Figure 4-9 illustrates a simulated instance of the PWM generator for the boost circuit. The sampled voltage is compared with the set target voltage, in this case the set target voltage is 415 V, and the error is used to produce the PWM signal. The frequency of the output PWM signal depends on the configuration of the block ‘PWM Carrier-Wave’ in Figure 4-9.

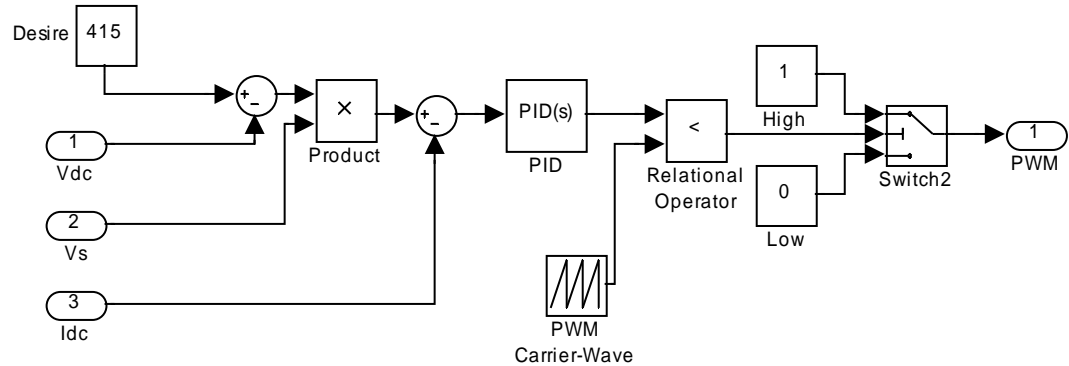
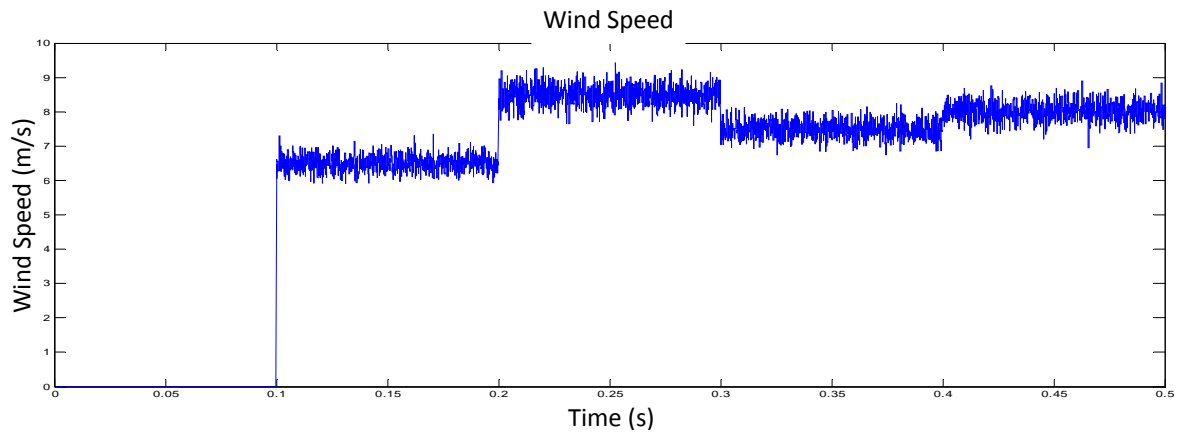


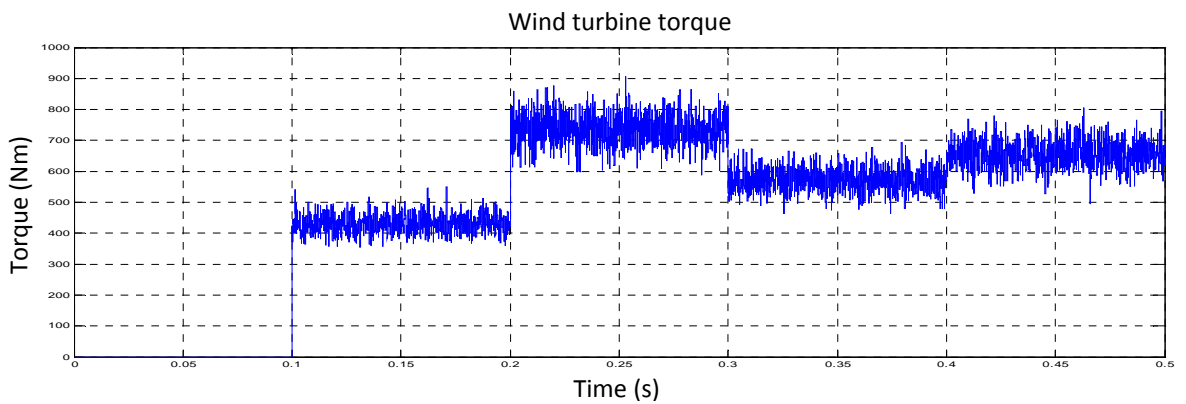
Figure 4- 9 Boost PWM generator model

4.6 The simulation results

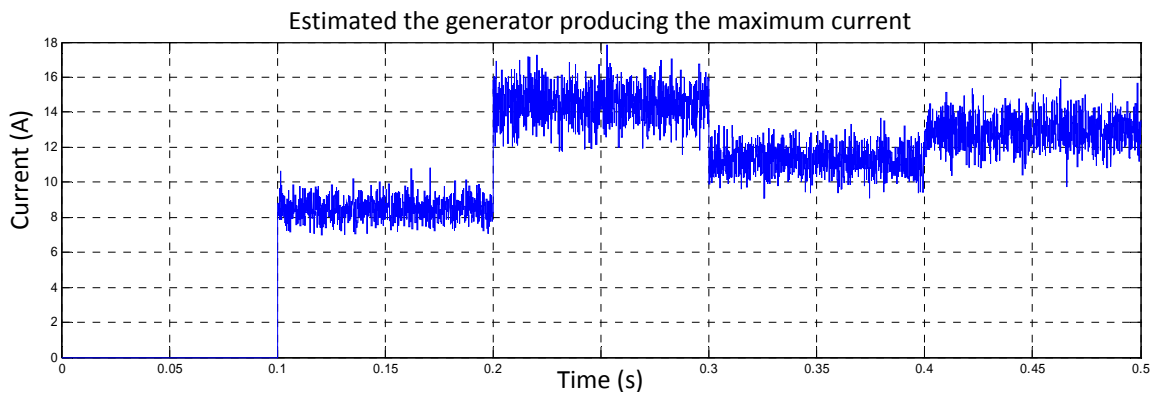
Figure 4-10 (a) shows a simulated wind resource, which is a multiple step wind speed (6.5 m/s, 8.5 m/s, 7 m/s and 7.5 m/s) with white noise input signal to the wind turbine PMSG, all the remaining simulation results are based on this wind resource input.



(a) Multiple step wind speed with white noise



(b) Wind turbine generator torque



(c) Estimated maximum DC current by MPPT

Figure 4- 10 Wind turbine output

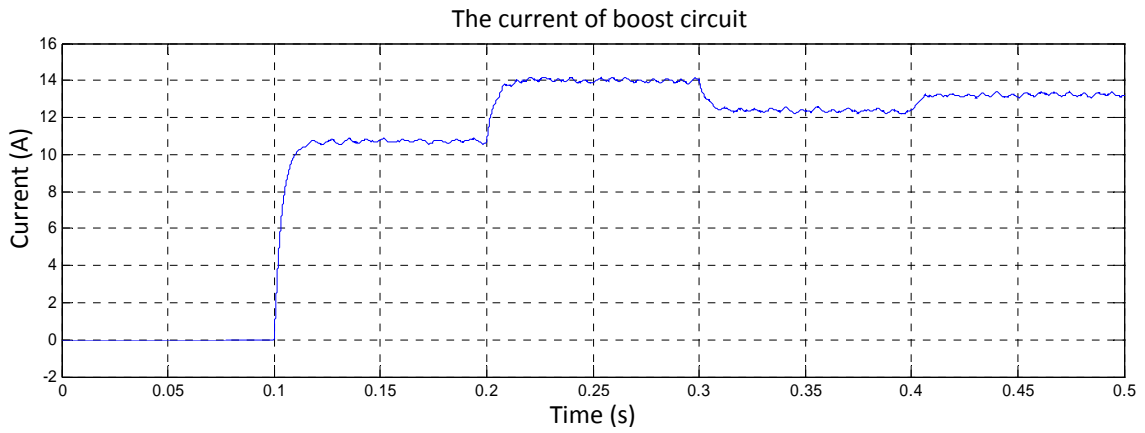


Figure 4- 11 Current flow through the inductor

Figure 4-11 shows the current flow through the inductor L_2 in Figure 4-8.

Figure 4-12 illustrates a simulated symmetrical 3-phase AC voltage output from the wind turbine PMSG, which is the 3-phase AC voltage source input to the AC/DC converter.

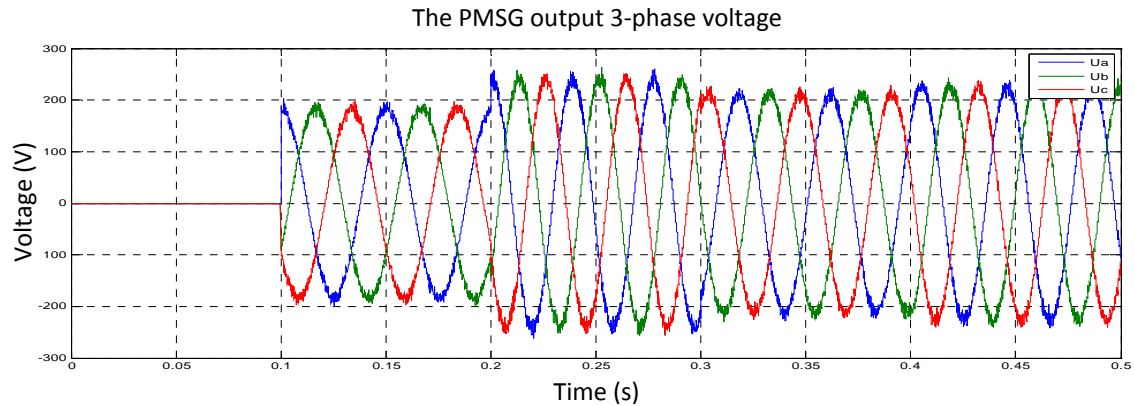


Figure 4- 12 3-phase AC voltage output from PMSG

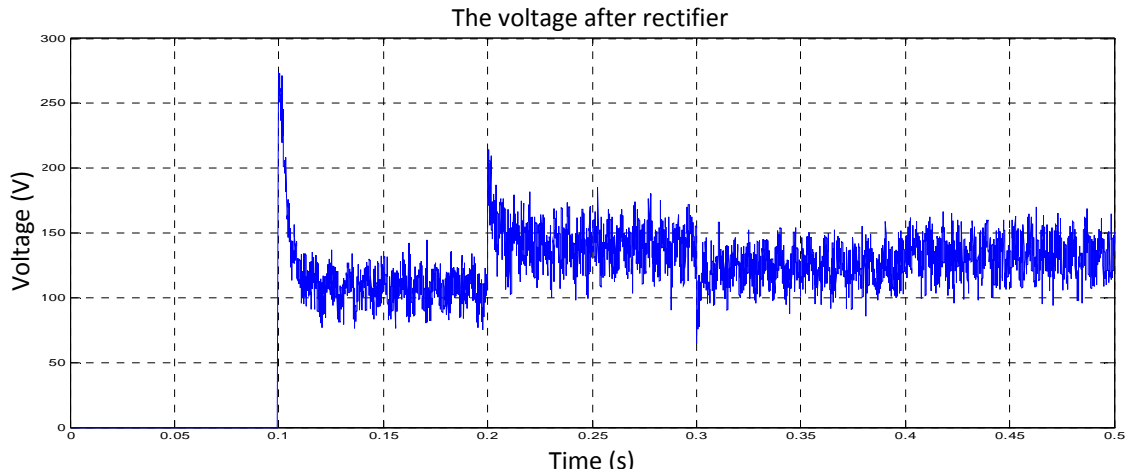


Figure 4- 13 Rectifier bridge output voltage

Figure 4-13 shows the voltage output of the rectifier bridge, the range of fluctuation of waveform is very significant with different wind speed, and the amplitude of peak to peak variations reaches approximately 60 V with the random variations superimposed on the constant nominal wind speed.

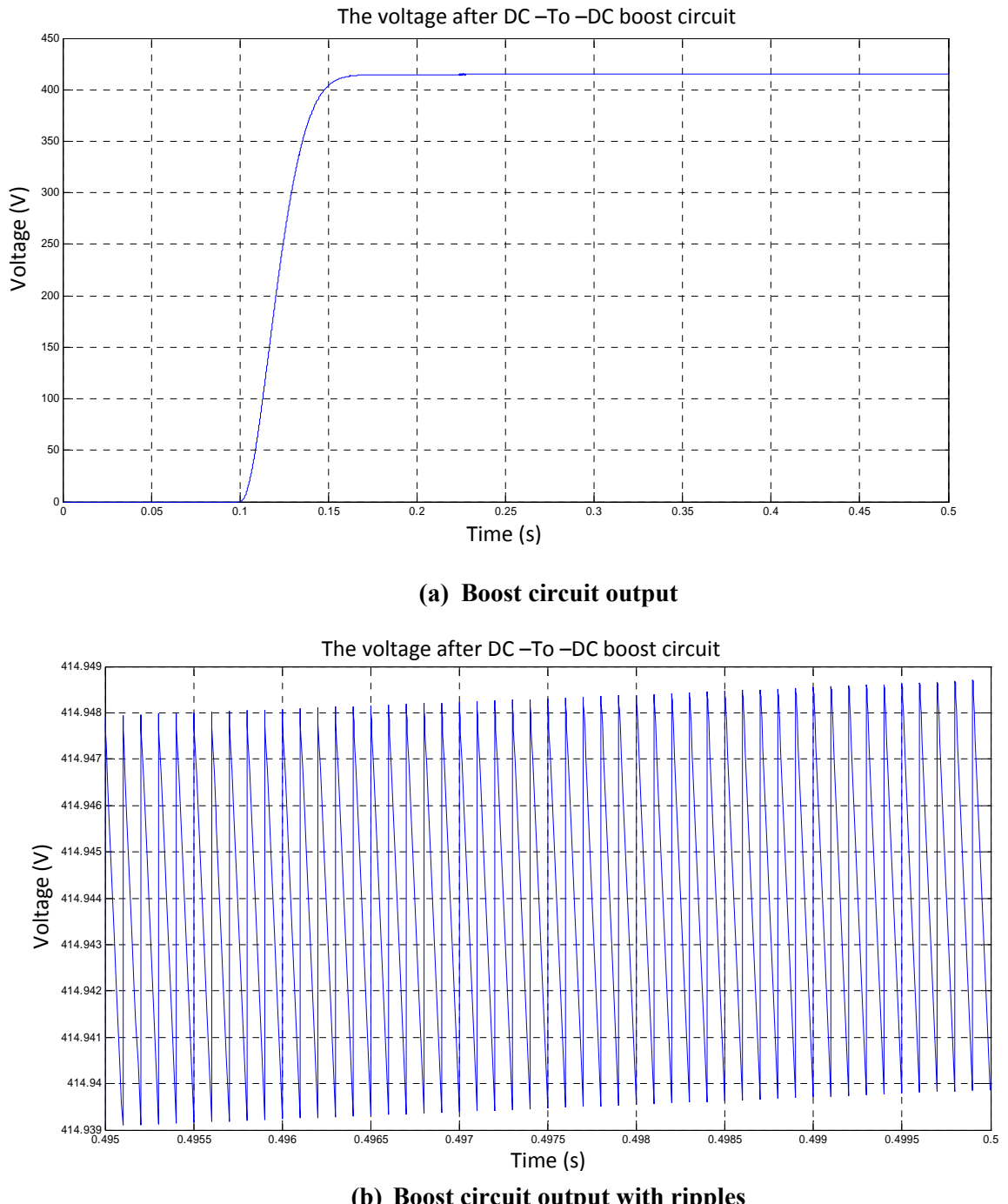


Figure 4- 14 DC voltage output from the boost circuit

Figure 4-14 shows the DC voltage output of the boost chopper circuit, based on the rectifier bridge output voltage waveforms in Figure 4-13. The figure (b) shows that the

DC output from boost chopper circuit with slight ripples, and the ripples in the range less than 15 mv, it is always maintains stable even with the fluctuation of the generator output of either amplitude or frequency. Even when the input AC voltage experiences large fluctuations and the generator output voltage is less than the grid voltage.

4.7 Summary

This chapter presents both the mathematical and simulation models of AC/DC rectifier, using diodes, and a boost circuit. The boost chopper circuit serves for both MPPT of the wind turbine generator control and the DC bus voltage stabilisation.

The simulation results demonstrate that the boost circuit provides MPPT for the wind turbine generator, and at the same time it maintains the setting voltage 415V, which is the input voltage source to the IGBT inverter.

It proves that the proposed diode rectifier circuit and the boost chopper circuit can be employed in PMSG for variable-speed wind turbines for both grid connection and battery charging.

Chapter 5 Inverter Modelling

5.1 Introduction

For the DC to AC inverter, according to its AC output waveforms, those topologies can be considered as voltage source inverters (VSI), where the independently controlled AC output is a voltage waveform. Similarly, those topologies can be found as current source inverter (CSI), where the independently controlled AC output is a current waveform (Espinoza J.R. 2001). There are a number of methods and techniques which are widely utilized to implement Voltage Source Inverters (VSIs). According to the carrier wave of PWM, the methods are classified into many types, such as Square-wave Operation, Carrier-based PWM, SFO-PWM, Regular and Non-regular Sampled PWM, Voltage Space Vector PWM (SVPWM) (Espinoza J.R. 2001). The major disadvantage of SVPWM is complicated calculation which demands considerable times. However, with rapid development of computer technology, the-state-of-the-art processor has reached nano-second level instruction cycle, and the above disadvantage is no longer a critical problem. Therefore the technique of SVPWM has been widely employed in many applications. An inverter implemented with SVPWM has the characteristics of low switching losses, high efficiency, high power factor and reduced harmonic effect, and many others. Therefore this project employs SVPWM for the development of the inverter model.

5.2 The SVPWM algorithm

Figure 5-1 illustrates the SVPWM algorithm, which works in a real time system. As the figure shows, the algorithm of the space vector pulse width modulation primarily consists of the following blocks: Identify sector, Locked phase, Calculate firing time, Carrier-wave, Triangular modulated wave and SVPWM.

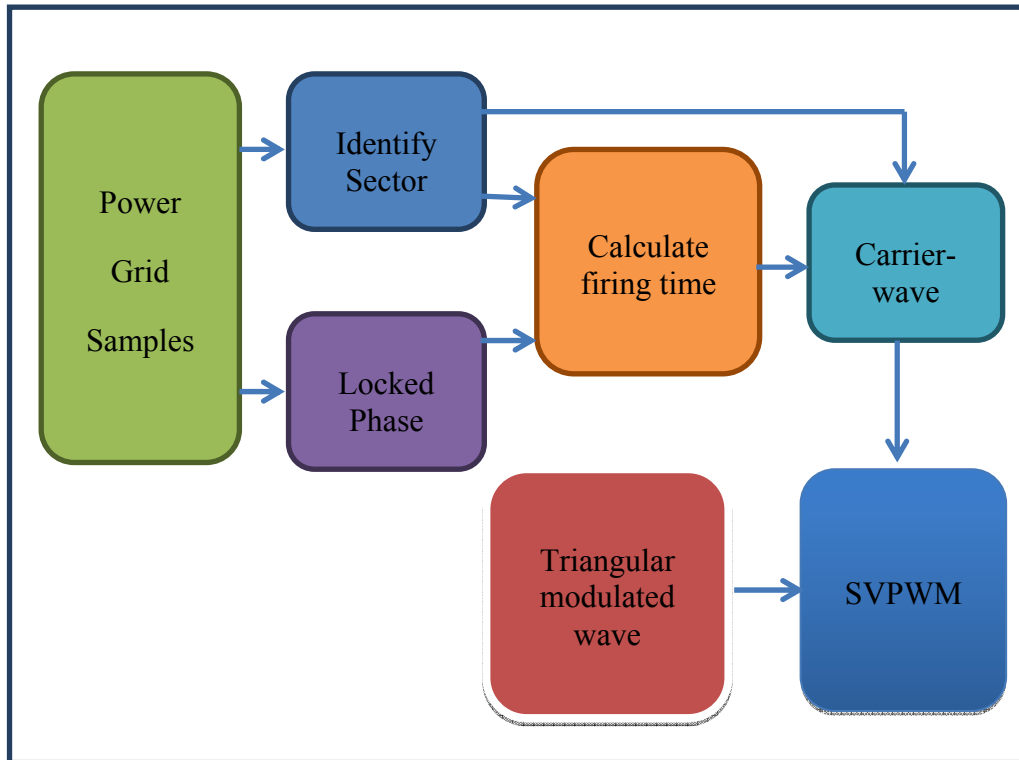


Figure 5 - 1 Framework of SVPWM algorithm

In the SVPWM algorithm, the period of a sinusoidal wave is divided into six sectors, and the size of each sector is $\pi/3$ radians. According to the sampling of the instantaneous grid voltage, the control system can determine the sector, in which the grid is working, and at the same time obtain the phase value of grid power.

Based on the present sector number and the phase value, the system calculates the firing time for IGBTs in the inverted bridge. The carrier waves are produced by the firing time and sector number, which is compared with the triangular modulated wave to generate SVPWM signals.

5.2.1 The principle of SVPWM

Figure 5-2 illustrates a common topology of inverter, which consists of an upper bridge (S1, S3, S5) and a lower bridge (S4, S6, S2).

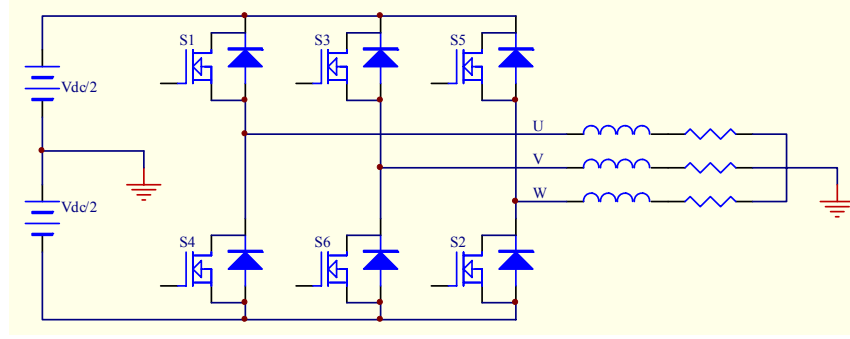


Figure 5 - 2 The topology of inverter

Each of the IGBT pairs in the upper and lower bridges cannot be conducting at the same time otherwise the power input will be shorted. Therefore the switching state of the upper bridge has to be opposite to that of the lower bridge.

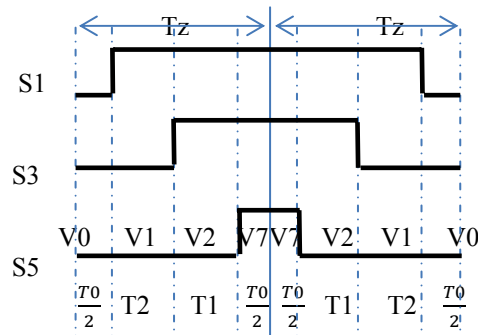
To focus on the upper bridge S1, S3 and S5, if logic ‘1’ indicates the switched on state and ‘0’ represents switched off state, the three switches have eight state combinations as listed in Table 5-1.

In order to reduce the switching times of the IGBT pair in the inverter and to reduce the effects of harmonics, the switching state of IGBT pairs are only changed once within a pulse period.

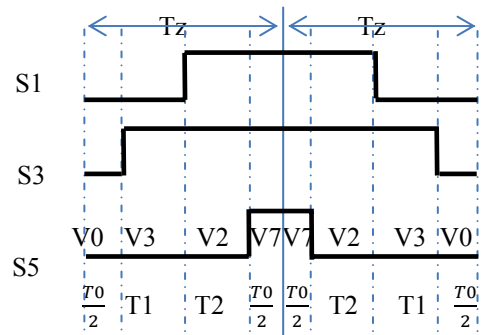
Vector	S5	S3	S1	V_u	V_v	V_w
V_0	0	0	0	0	0	0
V_1	0	0	1	$2V_{dc}/3$	$-V_{dc}/3$	$-V_{dc}/3$
V_2	0	1	1	$V_{dc}/3$	$V_{dc}/3$	$-2V_{dc}/3$
V_3	0	1	0	$-V_{dc}/3$	$2V_{dc}/3$	$-V_{dc}/3$
V_4	1	1	0	$-2V_{dc}/3$	$V_{dc}/3$	$V_{dc}/3$
V_5	1	0	0	$-V_{dc}/3$	$-V_{dc}/3$	$2V_{dc}/3$
V_6	1	0	1	$V_{dc}/3$	$-2V_{dc}/3$	$V_{dc}/3$
V_7	1	1	1	0	0	0

Table 5- 1 The relationship between work mode and phase voltage

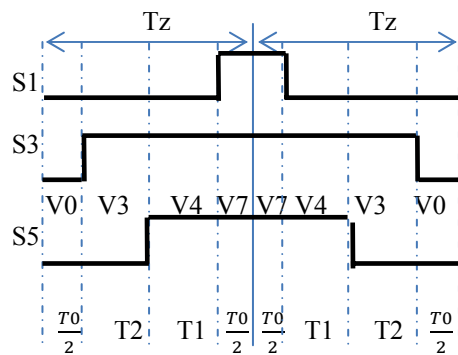
Table 5-1 illustrates that a 3-phase AC power can be synthesized by eight vectors, in which there are two zero vectors V_0 and V_7 . As illustrated by Figure 5-3 a period of the output voltage is divided into 6 patterns, the patterns show the switching state of the upper bridge IGBTs. Because the states of lower bridge are opposite to the upper bridge, the PWM signals of the lower bridge can be obtained by inverting the PWM signals of the upper bridge, therefore only the upper bridge control signal are shown in the following diagram.



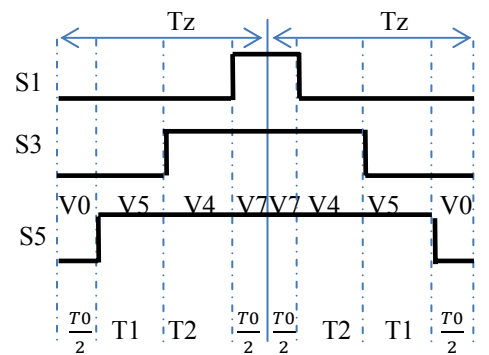
(a) Sector I switching state



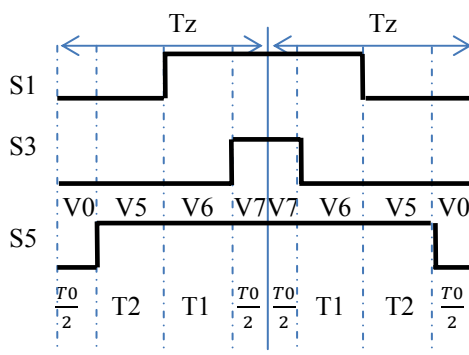
(b) Sector II switching state



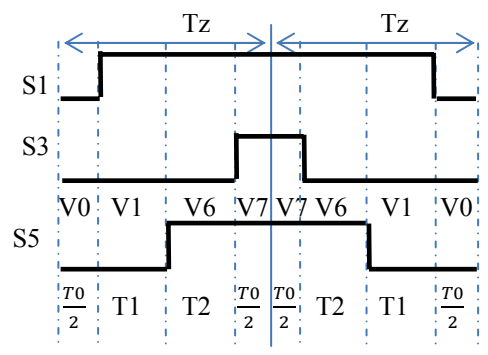
(c) Sector III switching state



(d) Sector IV switching state



(e) Sector V switching state



(f) Sector VI switching state

Figure 5 - 3 The patterns of voltage vectors

Taken from (Cai Mingfa 2006)

5.2.2 Clarke Transform

The voltage of each phase in a balanced 3-phase system can be represented with the following equation:

$$\begin{aligned} v_a &= v_{max} \cos \omega t \\ v_b &= v_{max} \cos(\omega t - 120^\circ) \\ v_c &= v_{max} \cos(\omega t - 240^\circ) \end{aligned} \quad (5-1)$$

where v_{max} is the amplitude of fundamental wave, $\omega = 2\pi f$, which is angular velocity.

Let

$$v_d = v_a = v_{max} \cos \omega t$$

$$v_q = v_{max} \sin \omega t$$

Then the equation (5-1) could be substituted with v_d, v_q as:

$$\begin{aligned} v_a &= v_d \\ v_b &= v_{max} (\cos \omega t \cos 120^\circ + \sin \omega t \sin 120^\circ) \\ &= -\frac{1}{2} v_d + \frac{\sqrt{3}}{2} v_q \\ v_c &= v_{max} (\cos \omega t \cos 120^\circ - \sin \omega t \sin 120^\circ) \\ &= -\frac{1}{2} v_d - \frac{\sqrt{3}}{2} v_q \end{aligned} \quad (5-2)$$

Therefore

$$\begin{bmatrix} v_a \\ v_b \\ v_c \end{bmatrix} = \begin{bmatrix} 1 & 0 \\ -1/2 & \sqrt{3}/2 \\ -1/2 & -\sqrt{3}/2 \end{bmatrix} \begin{bmatrix} v_d \\ v_q \end{bmatrix} \quad (5-3)$$

The equation (5-3) reveals that the voltage of 3-phase system could be represented as a space vector \dot{V} , where $\dot{V} = v_d + jv_q$.

The v_d, v_q can be obtained from the equation (5-3) as:

$$\begin{bmatrix} v_d \\ v_q \end{bmatrix} = \frac{2}{3} \begin{bmatrix} 1 & -1/2 & -1/2 \\ 0 & \sqrt{3}/2 & -\sqrt{3}/2 \end{bmatrix} \begin{bmatrix} v_a \\ v_b \\ v_c \end{bmatrix} \quad (5-4)$$

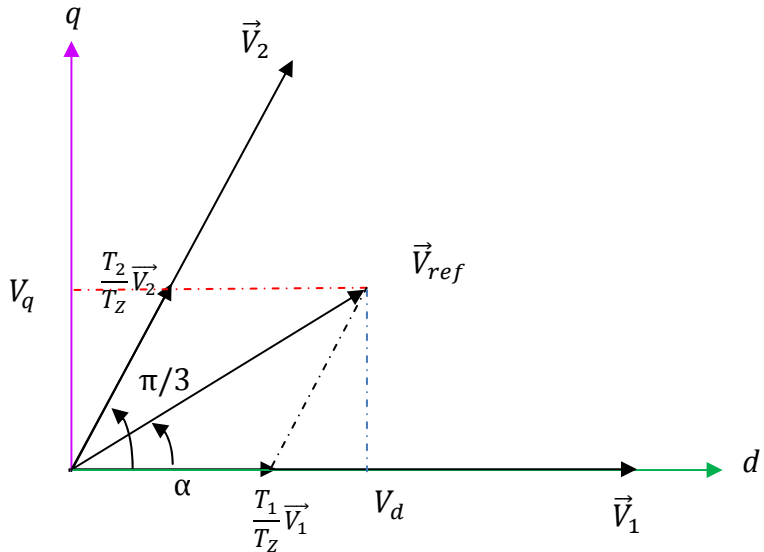


Figure 5 - 4 Cartesian to polar coordinates

According to the rule of the conversion from Cartesian to polar coordinates, the electromagnetic angle can be found from the Figure 5 - 4 as

$$\alpha = \arctg \left(\frac{V_q}{V_d} \right) \quad (5-5)$$

5.2.3 Identification

The Figure 5 - 5 illustrates the characteristic of sinusoidal waves of a 3-phase system. The period of sinusoidal waves of 3-phase is considered as 6 sectors, which are divided at the critical points of 1.0472 ($\pi/3$), 2.0944 ($2\pi/3$), 3.1416 (π), 4.1888 ($4\pi/3$), 5.236 ($5\pi/3$) and 6.2832 (2π) radians.

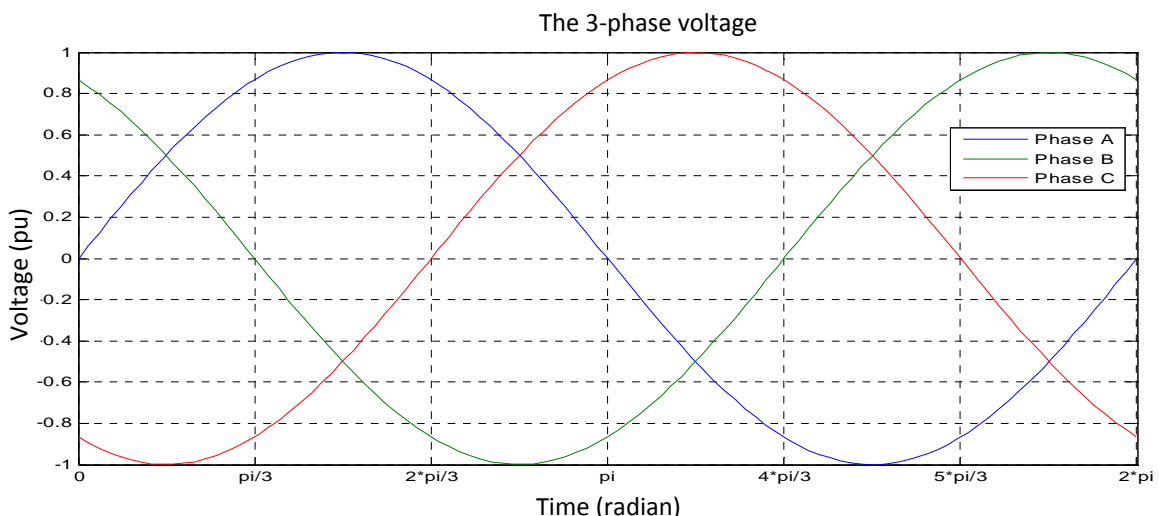


Figure 5 - 5 The sinusoidal waves of three phase

In the Figure 5 - 5, the blue, green and red lines indicate A-neutral, B-neutral and C-neutral voltages in a 3-phase balanced system. Analysis of the figure reveals the following table.

Sector	Areas	Phase A	Phase B	Phase C
1	$0 - \pi/3$	1	1	0
2	$\pi/3 - 2\pi/3$	1	0	0
3	$2\pi/3 - \pi$	1	0	1
4	$\pi - 4\pi/3$	0	0	1
5	$4\pi/3 - 5\pi/3$	0	1	1
6	$5\pi/3 - 2\pi$	0	1	0

Table 5- 2 The relationship between phase angle and phase neutral voltage

Note: In Table 5-2, the digit 1 is representative of the corresponding phase amplitude being greater than or equal to 0, the digit 0 expressing the amplitude is less than 0.

For the neutral voltage of Phase A, B and C, in this interpretation of the logical relationship an alternative method of expressing the relationship in algebra, is:

$$N = A + 2B + 4C \quad (5-6)$$

According to the equation (5-6), Table 5-2 is modified as follows.

Sector	Areas	Phase A	Phase B	Phase C	N
1	$0 - \pi/3$	1	1	0	3
2	$\pi/3 - 2\pi/3$	1	0	0	1
3	$2\pi/3 - \pi$	1	0	1	5
4	$\pi - 4\pi/3$	0	0	1	4
5	$4\pi/3 - 5\pi/3$	0	1	1	6
6	$5\pi/3 - 2\pi$	0	1	0	2

Table 5- 3 The relationship of sector mapping

5.2.4 Calculate firing time for IGBT switches

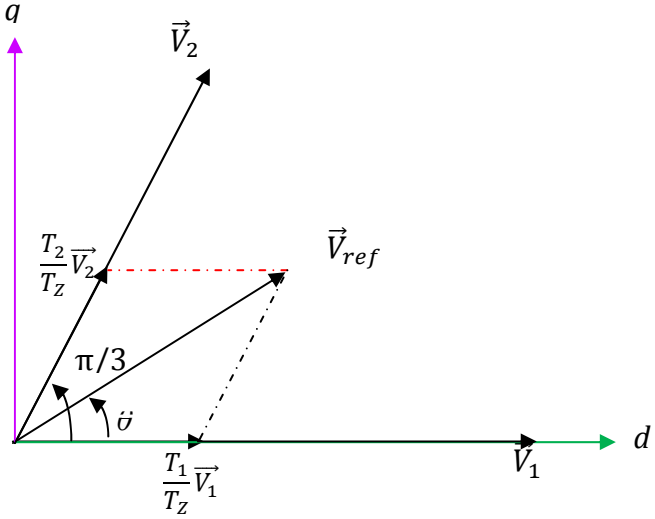


Figure 5 - 6 Vector synthesis schematic in sector 1

As Figure 5 - 6 illustrates the vectors located in sector 1, assuming T_z is the unit of time.

According to the Figure 5-6, the time T_1 and T_2 are obtained as follows:

$$\frac{|\vec{V}_{ref}|}{\sin\left(\frac{2\pi}{3}\right)} = \frac{|\vec{V}_1|T_1}{\sin\left(\frac{\pi}{3}-\theta\right)} \quad (5-7)$$

$$\frac{|\vec{V}_{ref}|}{\sin\left(\frac{2\pi}{3}\right)} = \frac{|\vec{V}_2|T_2}{\sin(\theta)} \quad (5-8)$$

Because of

$$|\vec{V}_1| = |\vec{V}_2| = |V_{dc}|$$

Therefore

$$T_1 = \frac{|\vec{V}_{ref}|}{|\vec{V}_1|} \frac{\sin\left(\frac{\pi}{3}-\theta\right)}{\sin\left(\frac{2\pi}{3}\right)} = M \sin\left(\frac{\pi}{3}-\theta\right) \quad (5-9)$$

$$T_2 = \frac{|\vec{V}_{ref}|}{|\vec{V}_1|} \frac{\sin \theta}{\sin\left(\frac{2\pi}{3}\right)} = M \sin \theta \quad (5-10)$$

$$T_0 = T_z - T_1 - T_2 \quad (5-11)$$

where M is the ratio of modulation, T_0 is the dead time of inverter.

$$M = \frac{2}{\sqrt{3}} \frac{|\vec{V}_{ref}|}{|V_{dc}|} \quad (5-12)$$

5.2.5 The over modulation

In theory, the calculation of the firing time for switching on and off the IGBT does not cause any problems. However, in a practical application the calculations can result in errors causing over modulation due to the following reasons.

- The algorithm requires division operations with rounding up in a practical application.
- Calculating the values of the function of *sine* and *cosine* will introduce rounding up errors producing some deviations.
- Calculations across the boundary of sectors may result in errors.

Therefore, in order to solve the problem of over modulation the linear modulation and non-linear modulation are employed to control over modulation.

If the module is working with dead time (T_0) greater than or equal to 0, equations (5-9), (5-10) and (5-11) be executed, otherwise equations (513), (5-14) and (5-15), below, will be executed.

$$T_1' = \frac{T_1}{T_1+T_2} T_z \quad (5-13)$$

$$T_2' = \frac{T_2}{T_1+T_2} T_z \quad (5-14)$$

$$T_0 = 0 \quad (5-15)$$

5.2.6 The principle of pulse width modulation

Figure 5-10 illustrates a simplest way to generate a pulse width modulation. A carrier wave (triangular waveform) is compared with a reference signal (sine wave). The state of output is positive value when the value of the reference signal is greater than the carrier waveform, otherwise it is negative value.

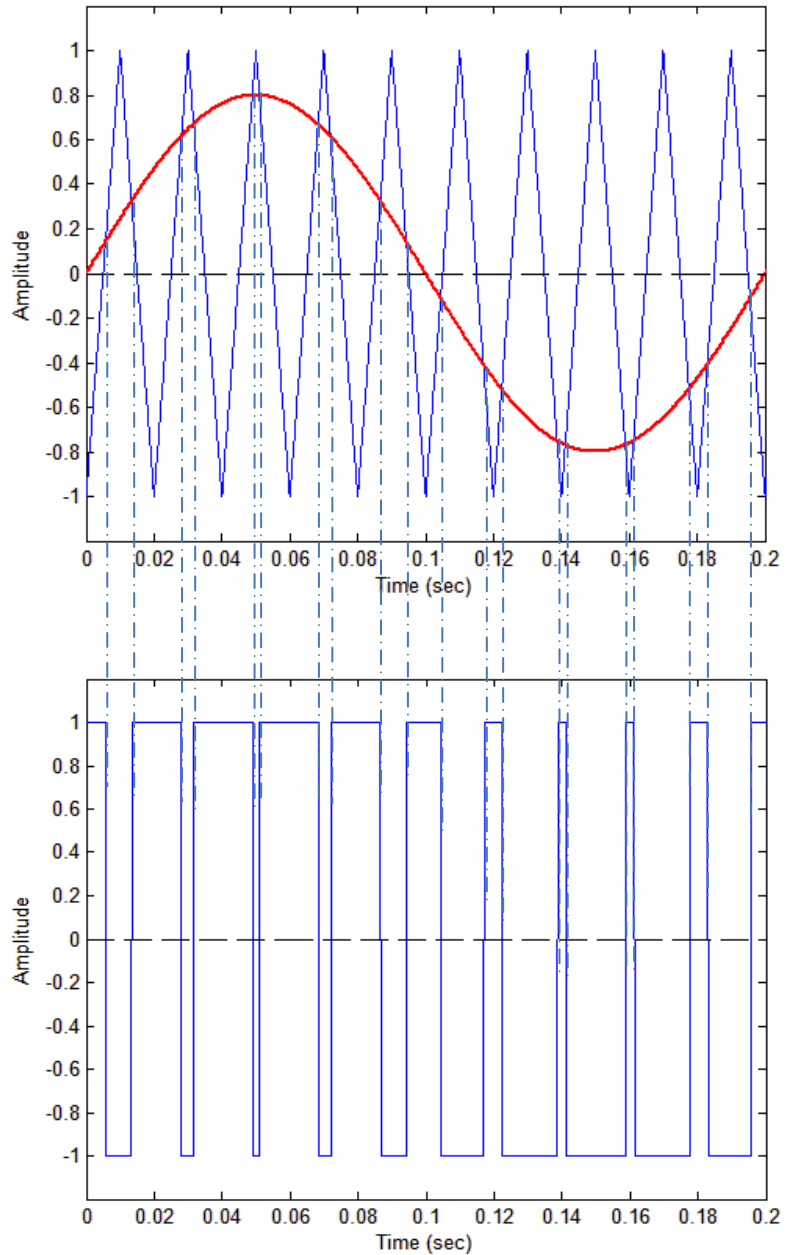


Figure 5 - 7 The principle of PWM generator

The output of a PWM generator can be described using:

$$V_{PWM} = \begin{cases} 1 & \text{if } V_{ref} \geq V_{tri} \\ -1 & \text{otherwise} \end{cases} \quad (5-22)$$

where

V_{PWM} is the value of PWM output

V_{ref} is the value of reference signal

V_{tri} is the value of triangular carrier wave

5.2.7 Carrier-wave of SVPWM

The fring time of each switch in the upper bridge for different sectors of the waveform can be obtained from Figure 5-3 using the following equations.

Sector I:

$$\begin{cases} F_{S1} = T_1 + T_2 + \frac{T_0}{2} \\ F_{S3} = T_2 + \frac{T_0}{2} \\ F_{S5} = \frac{T_0}{2} \end{cases} \Rightarrow \begin{bmatrix} F_{S1} \\ F_{S3} \\ F_{S5} \end{bmatrix} = \begin{bmatrix} 1 & 1 & 0.5 \\ 0 & 1 & 0.5 \\ 0 & 0 & 0.5 \end{bmatrix} \begin{bmatrix} T_1 \\ T_2 \\ T_0 \end{bmatrix} \quad (5-16)$$

Sector II:

$$\begin{cases} F_{S1} = T_1 + \frac{T_0}{2} \\ F_{S3} = T_1 + T_2 + \frac{T_0}{2} \\ F_{S5} = \frac{T_0}{2} \end{cases} \Rightarrow \begin{bmatrix} F_{S1} \\ F_{S3} \\ F_{S5} \end{bmatrix} = \begin{bmatrix} 1 & 0 & 0.5 \\ 1 & 1 & 0.5 \\ 0 & 0 & 0.5 \end{bmatrix} \begin{bmatrix} T_1 \\ T_2 \\ T_0 \end{bmatrix} \quad (5-17)$$

Sector III:

$$\begin{cases} F_{S1} = \frac{T_0}{2} \\ F_{S3} = T_1 + T_2 + \frac{T_0}{2} \\ F_{S5} = T_2 + \frac{T_0}{2} \end{cases} \Rightarrow \begin{bmatrix} F_{S1} \\ F_{S3} \\ F_{S5} \end{bmatrix} = \begin{bmatrix} 0 & 0 & 0.5 \\ 1 & 1 & 0.5 \\ 0 & 1 & 0.5 \end{bmatrix} \begin{bmatrix} T_1 \\ T_2 \\ T_0 \end{bmatrix} \quad (5-18)$$

Sector IV:

$$\begin{cases} F_{S1} = \frac{T_0}{2} \\ F_{S3} = T_1 + \frac{T_0}{2} \\ F_{S5} = T_1 + T_2 + \frac{T_0}{2} \end{cases} \Rightarrow \begin{bmatrix} F_{S1} \\ F_{S3} \\ F_{S5} \end{bmatrix} = \begin{bmatrix} 0 & 0 & 0.5 \\ 1 & 0 & 0.5 \\ 1 & 1 & 0.5 \end{bmatrix} \begin{bmatrix} T_1 \\ T_2 \\ T_0 \end{bmatrix} \quad (5-19)$$

Sector V:

$$\begin{cases} F_{S1} = T_2 + \frac{T_0}{2} \\ F_{S3} = \frac{T_0}{2} \\ F_{S5} = T_1 + T_2 + \frac{T_0}{2} \end{cases} \Rightarrow \begin{bmatrix} F_{S1} \\ F_{S3} \\ F_{S5} \end{bmatrix} = \begin{bmatrix} 0 & 1 & 0.5 \\ 0 & 0 & 0.5 \\ 1 & 1 & 0.5 \end{bmatrix} \begin{bmatrix} T_1 \\ T_2 \\ T_0 \end{bmatrix} \quad (5-20)$$

Sector VI:

$$\begin{cases} F_{S1} = T_1 + T_2 + \frac{T_0}{2} \\ F_{S3} = \frac{T_0}{2} \\ F_{S5} = T_1 + \frac{T_0}{2} \end{cases} \Rightarrow \begin{bmatrix} F_{S1} \\ F_{S3} \\ F_{S5} \end{bmatrix} = \begin{bmatrix} 1 & 1 & 0.5 \\ 0 & 0 & 0.5 \\ 1 & 0 & 0.5 \end{bmatrix} \begin{bmatrix} T_1 \\ T_2 \\ T_0 \end{bmatrix} \quad (5-21)$$

5.3 Modelling SVPWM using MATLAB/Simulink

Figure 5-8 illustrates the simulated in MATLAB/Simulink module based on the mathematical model described in Table 5-3. The simulation model is developed to determine the sector, in which the grid power is working, by the value of the instantaneous samples.

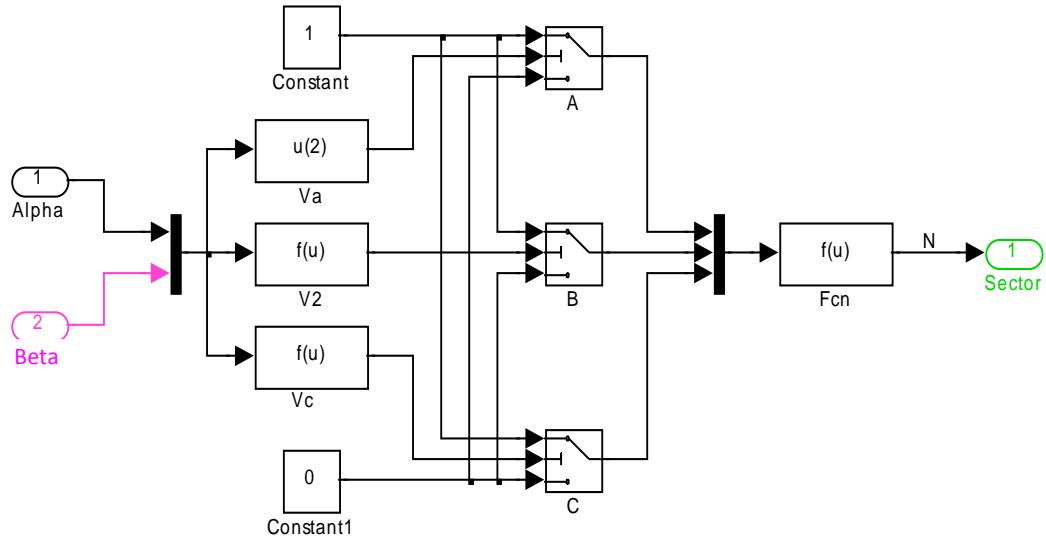


Figure 5 - 8 The module of sector identified with Simulink

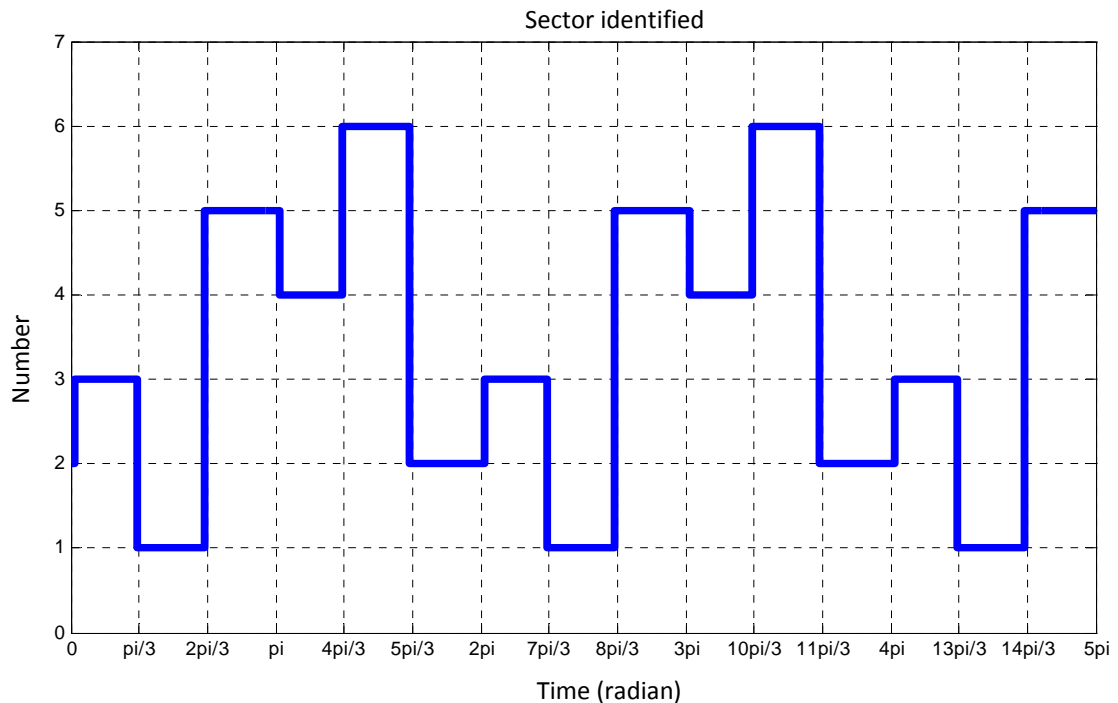


Figure 5 - 9 Simulation result of sector identified

Figure 5-9 shows that the results of this simulation identifying the sector match the results of analysis shown in Table 5-3.

Figure 5-10 is the model, created with MATLAB/Simulink, to put the sector numbers in order.

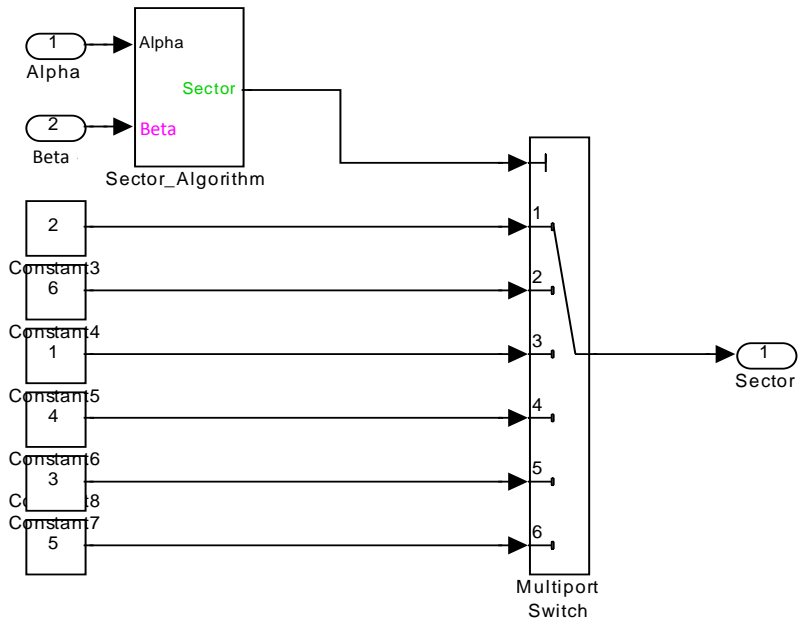


Figure 5 - 10 The modelling of converting sector number in order

The results shown in Figure 5-11 reveals that the model illustrated in Figure 5-10 has successfully identified the sectors.

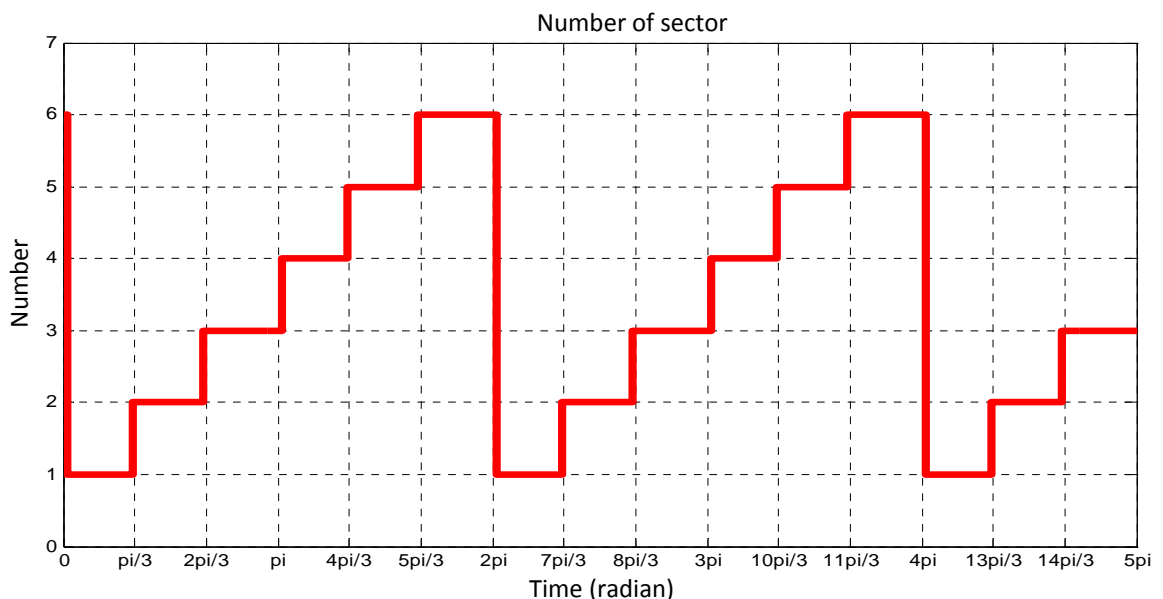


Figure 5 - 11 Result of converting sector number in order

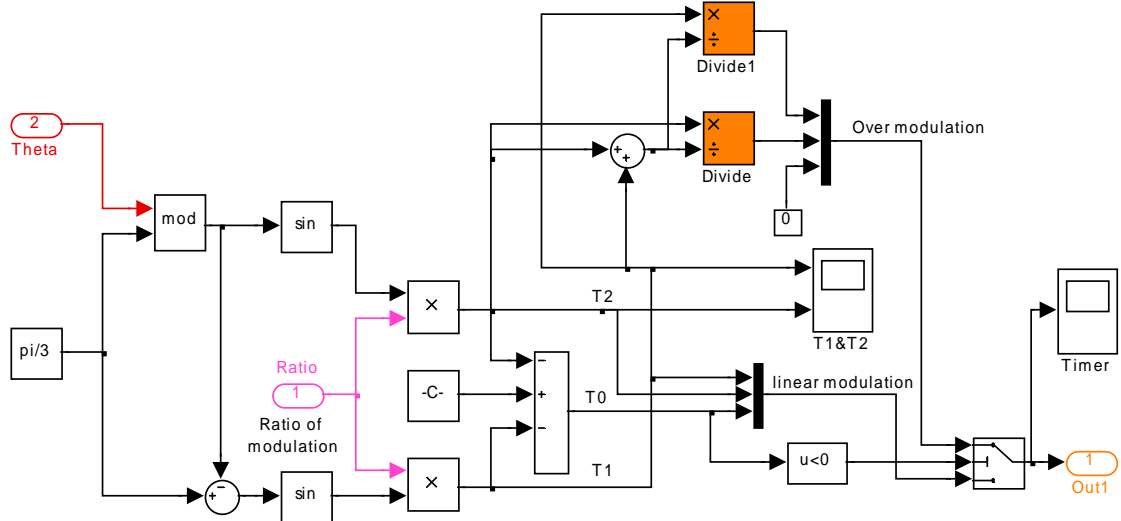


Figure 5 - 12 Modelling of firing time of IGBTs

Figure 5-12 illustrates a model based on the set of equations from (5-9) to (5-15). The model calculates the time of conduction for each active switching device. As the figure shows, the model has two inputs and one output, and these are the ratio of modulation, present phase angle and switching time respectively. The model is based on the input phase angle that calculates the switching time, and determines whether the routine to prevent over modulation is necessary to be executed.

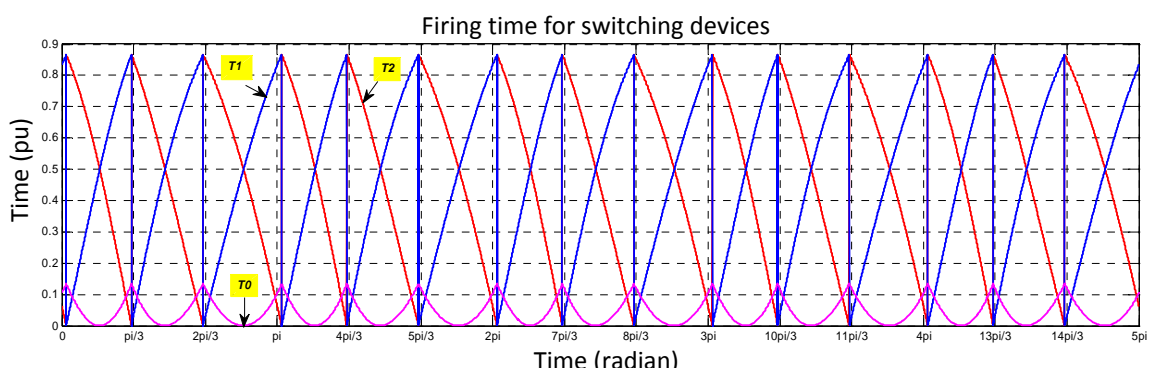


Figure 5 - 13 Firing time with over modulation

Figure 5-13 illustrates the resulting fring times with over modulation using the model shown in Figure 5-12. The red line, blue line and magenta line represent T_1 , T_2 and T_0 in the equation (5-9) to (5-11) respectively.

Figure 5-14 is a model created in MATLAB/Simulink based on equations (5-16) to (5-21).

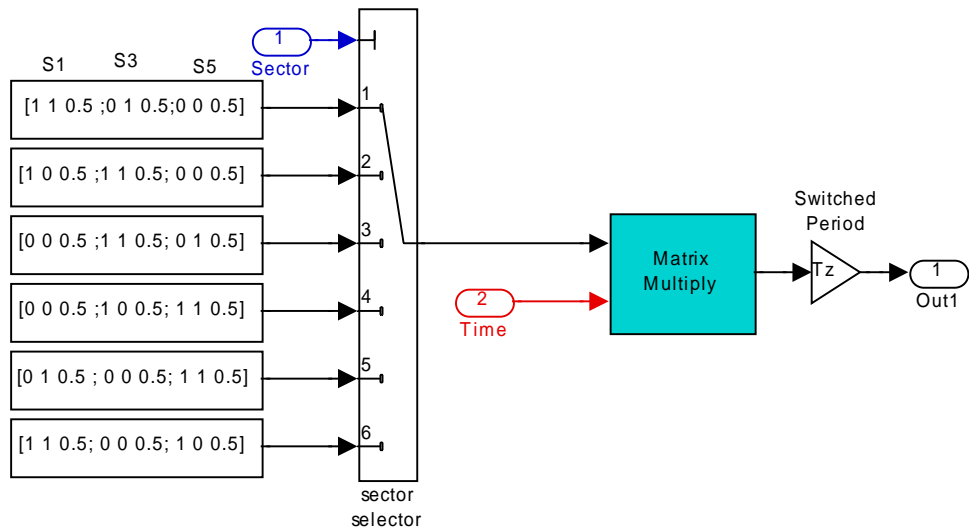


Figure 5 - 14 Modelling of generating carrier-wave in Simulink

Input signal ‘Time’ in the Figure 5-14 is a matrix variable. All calculations are based on per unit time before multiplying by the period of the PWM signal, so the output of the model has a gain of the switching period.

Figure 5-15 illustrates a set of carrier-waves produced from the output of the model shown in Figure 5-14. It is compared with a triangular wave to produce a set of PWM signals.

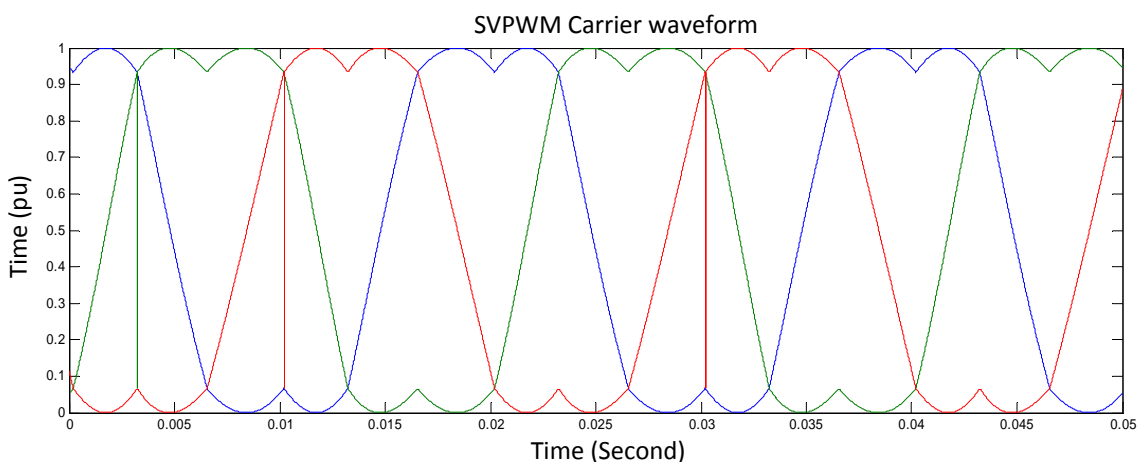


Figure 5 - 15 The reference waveform with SVPWM

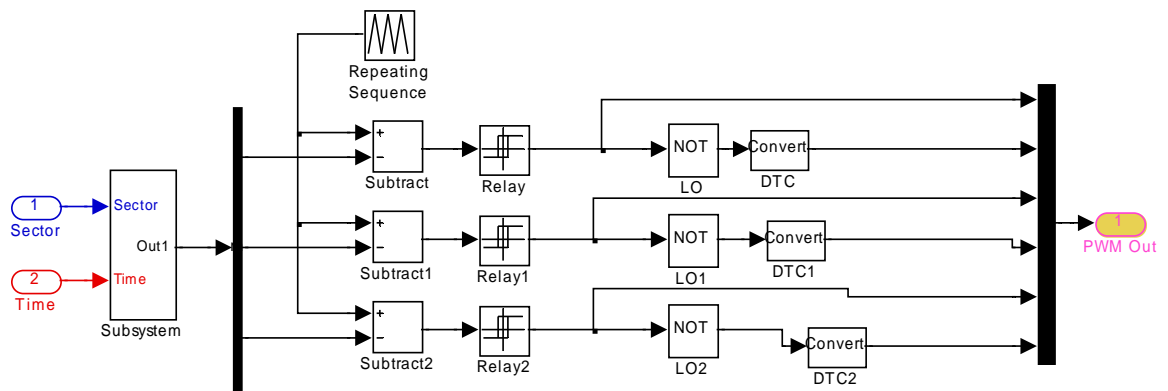


Figure 5 - 16 Modelling SVPWM

Figure 5-16 shows the model used to implement SVPWM according to the firing time of the upper bridge in the converter circuit illustrated in Figure 5-2.

In Figure 5-16, the frequency of triangular wave is 10 kHz, and the parameter of Repeating Sequence is configured as:

Time Values: [0 0.5 T_z T_z]

Output Values: [0 T_z 0]

where $T_z = 1\text{e-}4$ is the period of triangular wave.

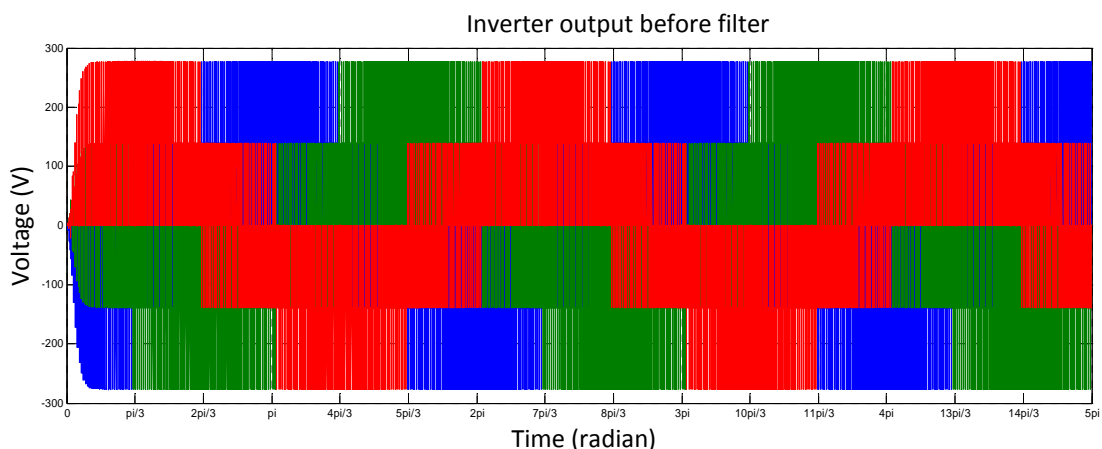


Figure 5 - 17 Output from inverter without filter

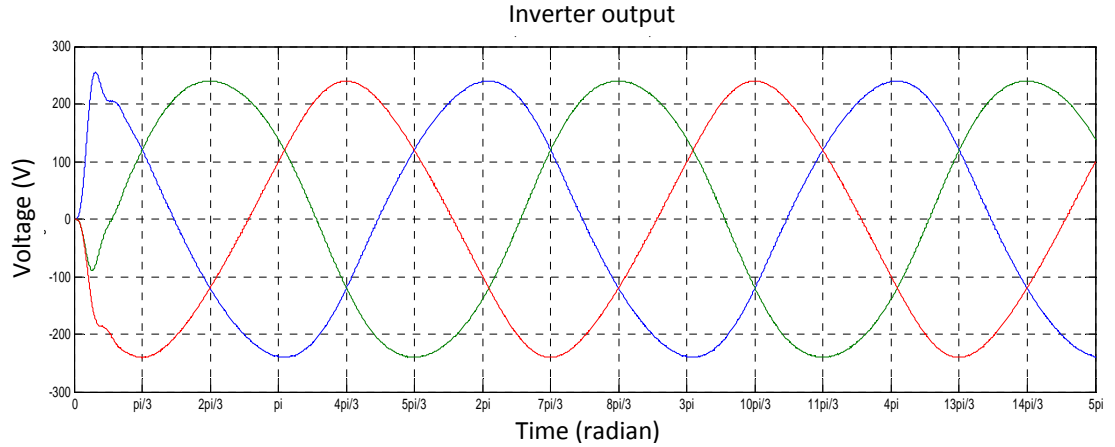


Figure 5 - 18 3-phase AC output from inverter

Figure 5-17 illustrates the result of inverter output without LC filter. Figure 5-18 shows the smoothed output from the inverter.

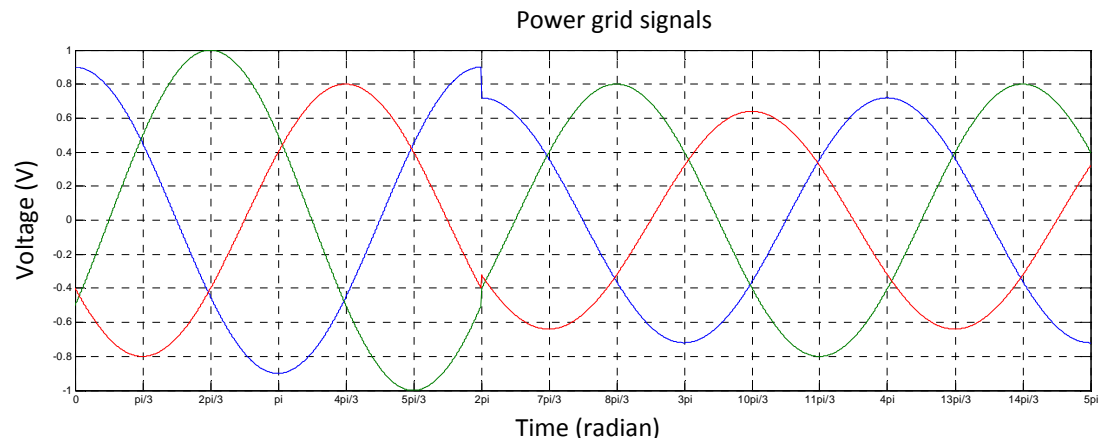


Figure 5 - 19 3-phase AC samples from power grid

Figure 5-19 is a simulated 3-phase AC power source, which are be used to provide simulated samples from the power grid for the modelling of the SVPWM. In order to simulate grid voltage sag, the power source offers a set of abnormal signals. The figure shows that phase A (blue line) starts with the amplitude drop by 10%, and phase C (red line) with a 20% drop. After one cycle all the signals are further dropped by 20% of their amplitude at the start.

5.4 Summary

The principles of an inverter based on SVPWM are presented in detail, and a number of mathematical models are given. An inverter based SVPWM system has been modelled using MATLAB/Simulink and Figure 5-17 and Figure 5-18 demonstrates that the SVPWM algorithm was successfully implemented.

Figure 5-19 shows that the grid power is with some voltage sag. If the voltage sag does not reach the “stop to output” condition, the inverter output still maintains stable output, which fulfils the low voltage ride through (LVRT) requirement chapter 6.

Chapter 6 Voltage Sag Detection

6.1 Low Voltage Ride Through

With the rapid growth of wind power generation, its impact on the power grid is increasing. In the past few decades, the most of wind turbine majorly were based on the Denmark's concept. Because induction generator is widely configured wind turbine, and the generator excited circuit directly connects to the power grid, as the power grid with disturbances and occurs voltage dips the generator loses excitation, which causes the wind turbine can not generate power. In this situation, the wind turbine should be tripped, otherwise, if the wind turbine still connects to the power grid, that leads to the voltage of the power grid can not be recovered(Chi Y.N. 2009). For this reason, new Grid Codes for wind power plants have been introduced in many countries, in which the low voltage ride through (LVRT) requirement for wind turbine grid connection has been enforced.

Wind energy is a random and intermittent resource, and wind speed is also unpredictable, that causes the wind plant transmits power with disturbances. The disturbances could potentially results in other wind farm's control system blackouts. On the other hand, as the power grid is with deep voltage sag the local power converter system should be safely protected (Abbey and Joos 2005).

The LVRT requirement is that the wind turbine must work properly should a low voltage fault occur. The LVRT requires actions to be taken by the wind turbine controller responding to the voltage sag ratio and the fault duration. Different countries or utilities present slightly different requirements in terms of the LVRT characteristic.

Figure 6.1 describes the LVRT characteristic in Germany (Shin H.J., et al. 2011), Figure 6.2 presents the LVRT characteristic for the Nordic countries Norway, Denmark and

Sweden (Molinas Marta, et al. 2008), and Figure 6.3 illustrates the LVRT curve from E.ON (Alepuz S., et al. 2010).

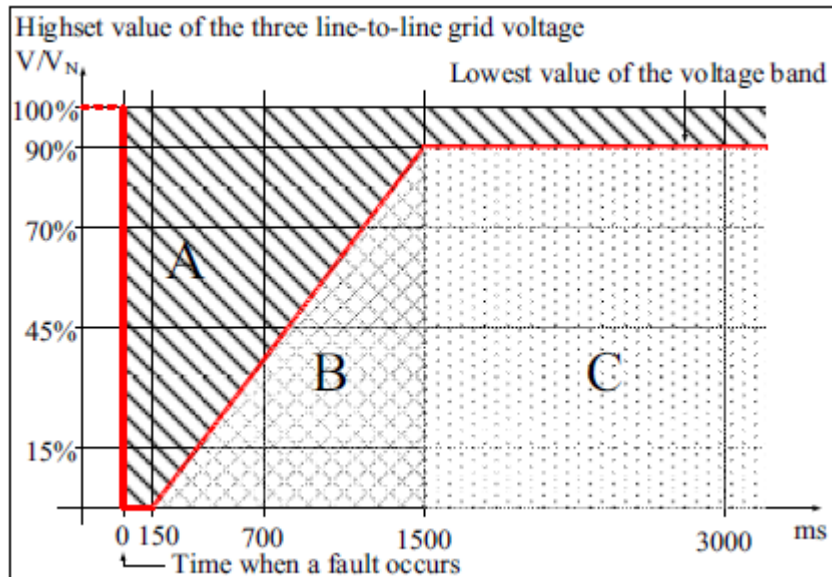


Figure 6- 1 LVRT limit curve in German grid code

Figure taken from (Shin H.J., et al. 2011)

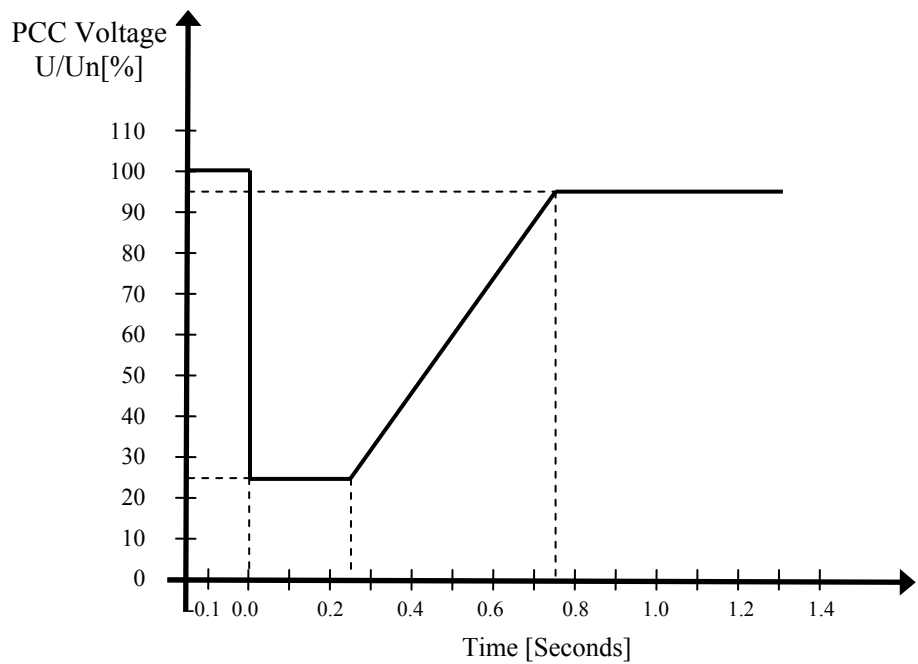


Figure 6- 2 LVRT curve from Nordel grid code

Figure taken from (Molinas Marta, et al. 2008)

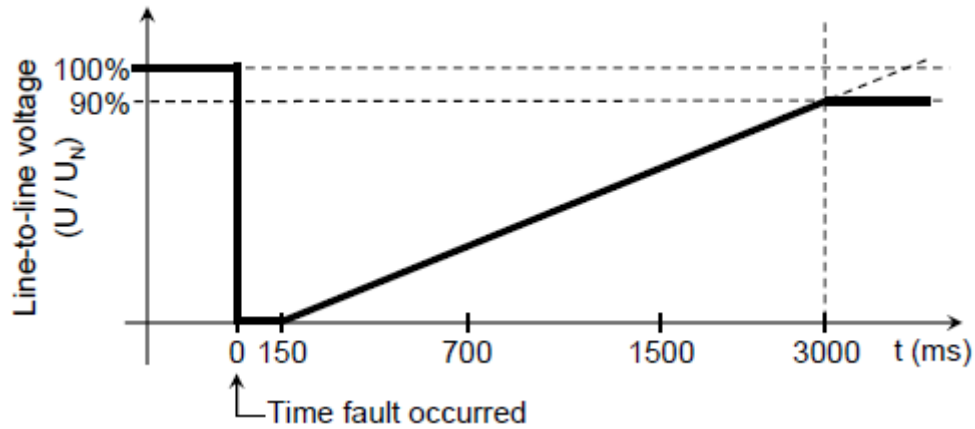


Figure 6- 3 LVRT curve from E.ON grid code

Figure taken from (Alepuz S., et al. 2010)

In order to ensure safe operation of the power grid network and implement the LVRT function for a wind power system, fast and accurate detection of a power grid voltage sag fault is of great importance.

6.2 Overview on power grid voltage sag detection methods

There are different power grid voltage sag detection methods which have been developed by researchers/engineers worldwide, and the conventional techniques include peak voltage detection (Chu H.Y., et al. 1992; Ding K., et al. 2006), mean value measurement, root mean square (RMS) detection (Deckmann S.M. and Ferrira A.A. 2002), DQ transform (Shin H.J., et al. 2011), $\alpha\beta$ transform, advanced $\alpha\beta$ transform (Lee Chia-Tse, et al. 2011), matrix method, Fourier transform(Yang W.R. and Yang W.X. 2010), etc.

In 2004, Chris Fitzer, Mike Barnes and Peter Green (Fitzer C., et al. 2004), presented a space vector method to detect the voltage sag and fluctuation of a power grid, that is well known as DQ detection. For the purpose of acquiring the amplitude of the grid, the strategy includes two mathematical transforms. One of the transforms is called Park transform, another is Clarke transform. The algorithm obtains the amplitude of voltage by means of DQ vectors. From the point of view of the operational speed, the algorithm

is complicated. The outcomes given in the paper show significant fluctuation when the power grid suffers asymmetric voltage sag and this is difficult detection.

The common characteristics of peak voltage detection, mean value measurement and RMS detection are easy to implement and fast. However these techniques experience some time delay at least one period of the voltage of the power grid.

Both DQ and $\alpha\beta$ transforms can rapidly and accurately monitor the grid voltage sag if all the three phases symmetrically (simultaneously) drop, however other forms of voltage dips, the outcome varies significantly.

Table 6-1 summarises the advantages and disadvantages of conventional voltage sag detection techniques.

Detection Methods	Advantages	Disadvantages
Peak Voltage	<ul style="list-style-type: none"> 1. Simple 2. Low computational cost 3. Easy implement 	<ul style="list-style-type: none"> 1. At least one cycle of AC power delay 2. Need 3 modules for 3-phase AC power grid
RMS	<ul style="list-style-type: none"> 1. Simple 2. Low computational cost 3. Easily implement 	<ul style="list-style-type: none"> 1. At least one cycle of AC power delay 2. Need 3 modules for 3-phase AC power grid
DQ transform	<ul style="list-style-type: none"> 1. Faster detection 2. Be able to real time detect 3-phase voltage symmetrically fall down 	Results with fluctuation as 3-phase voltage asymmetrically fall down

$\alpha\beta$ transform	Be able to detect voltage sag very well	Doing two times mathematical transmit: $abc/\alpha\beta, \alpha\beta/dq,$ Which means high computational cost
Matrix transform	Be able to detect voltage sag very well	Complicated mathematical computation: high computational cost
Fourier transform	Be able to detect voltage sag very well	Complicated mathematical computation: high computational cost

Table 6- 1 Comparison of conventional grid voltage detection techniques

From the point of view of the computational cost, executing the complex mathematical operation of matrix method and Fourier transform undoubtedly increases the computational cost of the controller.

With the exception of the matrix and Fourier transform methods, all methods discussed above are appropriate for the situation of 3-phase symmetrical voltage fall down. Therefore, for a complete system, it requires three detection modules, one for each phase, in order to accurately implement detection of asymmetric voltage sag. It undoubtedly increases the cost and complexity of system.

Due to the issues discussed above, it is of both practical and economic value to find a strategy for the controller with a simple and rapid mathematical algorithm to detect the 3-phase AC voltage sag.

The method proposed below is suitable for the detection of single phase, 2-phase or 3-phase symmetrical or asymmetrical voltage sags.

The author has developed a novel solution for fast, accurate detection of 3-phase AC power grid voltage sag and the solution is simpler and more universal than other techniques proposed by other researchers and/or used in the industry.

6.3 The mathematical model of a novel grid voltage sag detection

The symmetrical voltage of 3-phase grid can be expressed in mathematical equation as follows:

$$\begin{aligned} v_a &= v_{max} \cos \omega t \\ v_b &= v_{max} \cos(\omega t - \frac{2\pi}{3}) \\ v_c &= v_{max} \cos(\omega t + \frac{2\pi}{3}) \end{aligned} \quad (6-1)$$

Setting v_d and v_q as

$$\begin{aligned} v_d &= v_a = v_{max} \cos \omega t \\ v_q &= v_{max} \sin \omega t \end{aligned} \quad (6-2)$$

Hence, substituting into Equation (6-1),

$$\begin{aligned} v_a &= v_d \\ v_b &= v_{max} \left(\cos \omega t \cos \frac{2\pi}{3} + \sin \omega t \sin \frac{2\pi}{3} \right) \\ &= -\frac{1}{2} v_d + \frac{\sqrt{3}}{2} v_q \\ v_c &= v_{max} \left(\cos \omega t \cos \frac{2\pi}{3} - \sin \omega t \sin \frac{2\pi}{3} \right) \\ &= -\frac{1}{2} v_d - \frac{\sqrt{3}}{2} v_q \end{aligned} \quad (6-3)$$

The equation can be written in matrix format as below.

$$\begin{bmatrix} v_a \\ v_b \\ v_c \end{bmatrix} = \begin{bmatrix} 1 & 0 \\ -1/2 & \sqrt{3}/2 \\ -1/2 & -\sqrt{3}/2 \end{bmatrix} \begin{bmatrix} v_d \\ v_q \end{bmatrix} \quad (6-4)$$

v_d and v_q can be obtained through finding the inverse matrix of the constant matrix in the Equation (6-4).

$$\begin{bmatrix} v_d \\ v_q \end{bmatrix} = \frac{2}{3} \begin{bmatrix} 1 & -1/2 & -1/2 \\ 0 & \sqrt{3}/2 & -\sqrt{3}/2 \end{bmatrix} \begin{bmatrix} v_a \\ v_b \\ v_c \end{bmatrix} \quad (6-5)$$

Hence, the voltage RMS can be expressed as follows:

$$\begin{aligned} V &= v_{max} \\ &= \sqrt{v_{max}^2(\cos \omega t^2 + \sin \omega t^2)} \\ &= \sqrt{v_d^2 + v_q^2} \end{aligned} \quad (6-6)$$

where, v_{max} is the peak value of 3-phase voltage.

Analysis of Equation (6-5) shows that any change of 3-phase voltage will be feedback on the variable v_d .

In order to ensure that the v_d , v_q signals are synchronised in the Equation (6-2), v_q signal can be obtained by derivation of v_d .

$$\begin{aligned} \frac{d(v_d)}{dt} &= (v_{max} \cos \omega t)' \\ &= -v_{max} \omega \sin \omega t \\ &= -v_q \omega \end{aligned} \quad (6-7)$$

Hence

$$v_q = -\frac{d(v_d)}{dt} / \omega \quad (6-8)$$

where, ω is the angular frequency in rad/s.

In a practical application, the derivation of discrete values in unit time is the present sampling value minus the previous sample. Therefore, complicated derivative operation is simplified and become the operation of subtraction.

Because the right hand side of Equation (6-8) contains the derivative of v_d , the value of v_q probably is significantly large when the grid voltage fluctuates. Consequently, the output of derivative needs to be filtered. Because the continuous signals are without discontinuities, if the sampling rate is fast enough the delay introduced does not affect the control, it can be shifted by several sampling periods. The sample is not immediately output, the sample output when the sample data is continuously the same as previous samples for a predetermined sample count. However, there can be several instruction cycles of delay using the strategy above. With contemporary high speed processor several instruction cycles only take a few nanoseconds, which can be neglected when processing signals sampled at millisecond intervals. The flowchart of strategy is given as follows:

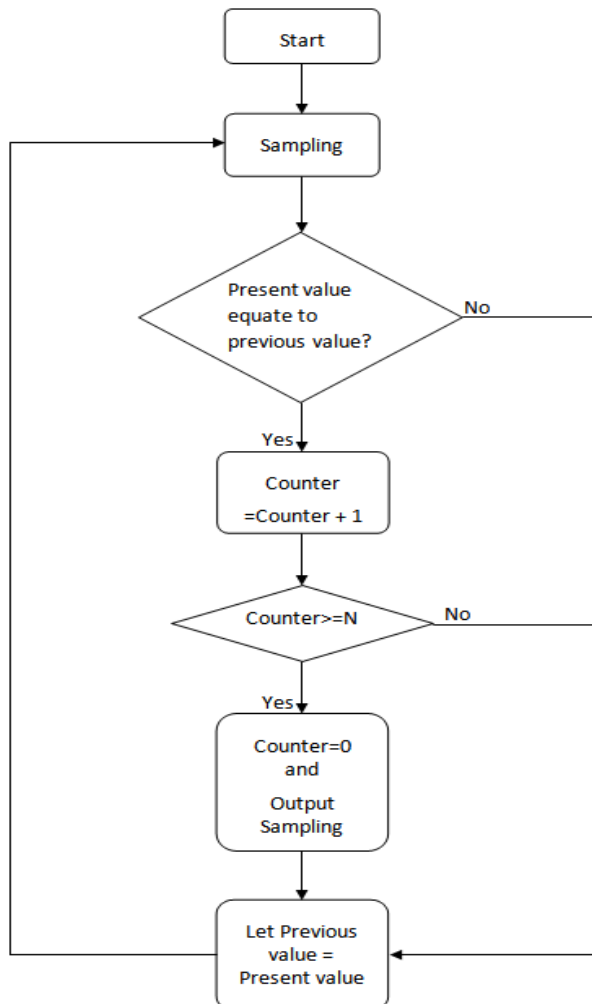


Figure 6- 4 The flowchart of filter algorithm

6.3 Modelling of voltage sag detection

Figure 6-5 shows a MATLAB/Simulink model of the voltage sag detector. The block labelled fluctuation in the model is a custom model. It is employed to allow the user to simulate a voltage source with the desired fluctuation. The figure shows that the model only utilises the v_d signal and the v_q signal is not used. The filter in the model is an s-builder block, which is used to implement the flowchart in Figure 6-4. A C program listing is given in Appendix D.

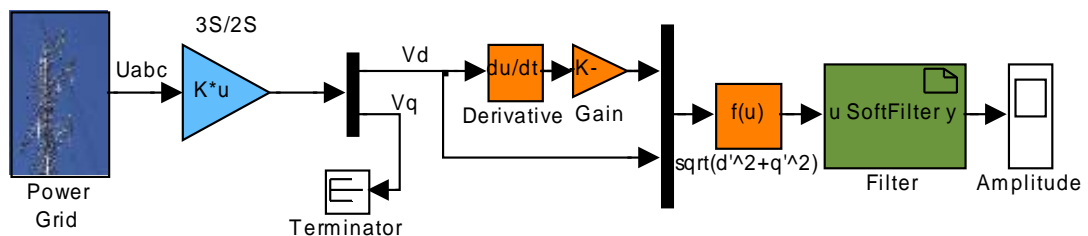
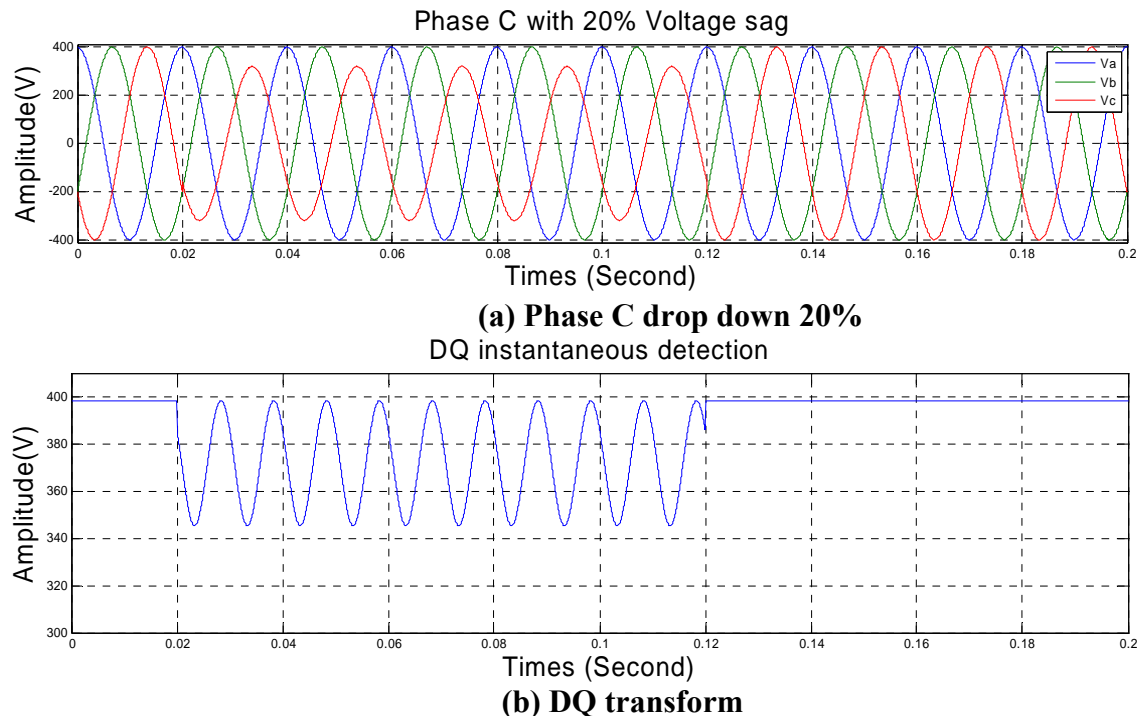


Figure 6-5 Model of the voltage sag detection

6.4 The simulation results

Figure 6-6 shows a comparison of the detection results obtained by using the DQ transform, mean value and the proposed new method.



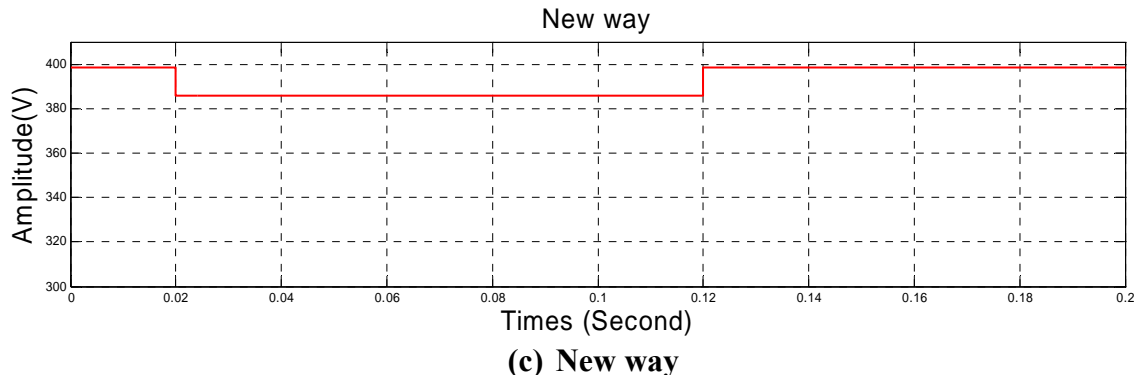


Figure 6- 6 Only phase C with 20% drop

In Figure 6-6 (a), phase C of the power source drops by 20%. The blue line in Figure 6-6 (b) is the detection result obtained by the DQ transform and shows significant oscillation. The red line in Figure 6-6 (c) is the outcome of using the new method to detect voltage sag, showing consistent and accurate detection. It obviously reveals that this method produces a delayed and stepped result.

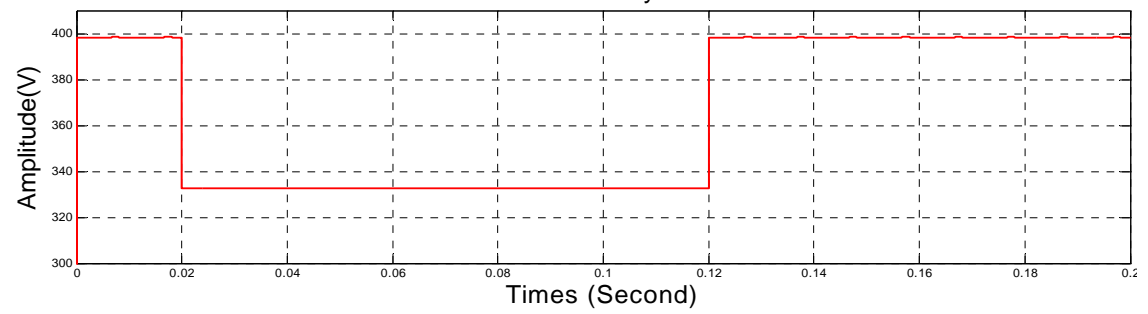
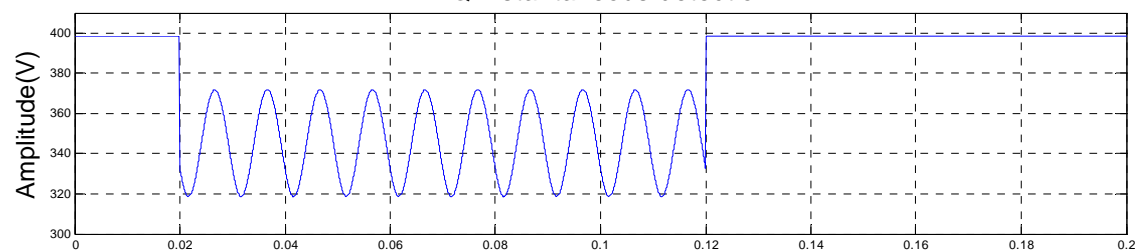
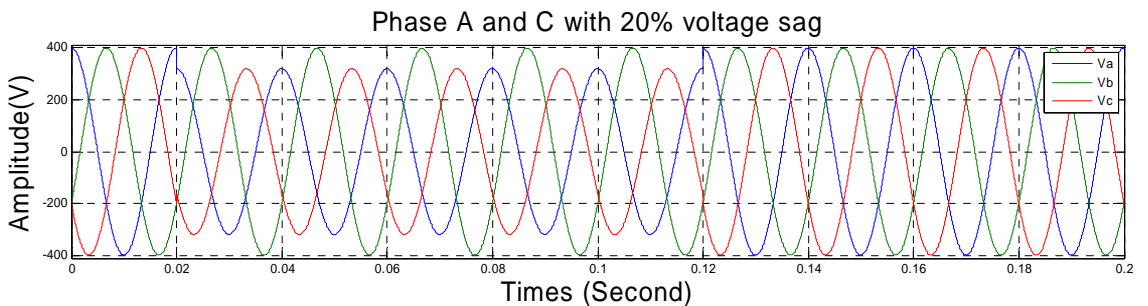


Figure 6-7 Both phase A and phase C with voltage sag

Figure 6-7 shows the results of another simulation in which both phase A and phase C drop by 20%. As the figure illustrates these results are consistent with the previous simulation.

Figure 6-8 shows the detection results produced when the grid is operated under normal conditions. The outcomes from the DQ transform and the new method overlap each other. It demonstrates that the new method works in the normal situation as well.

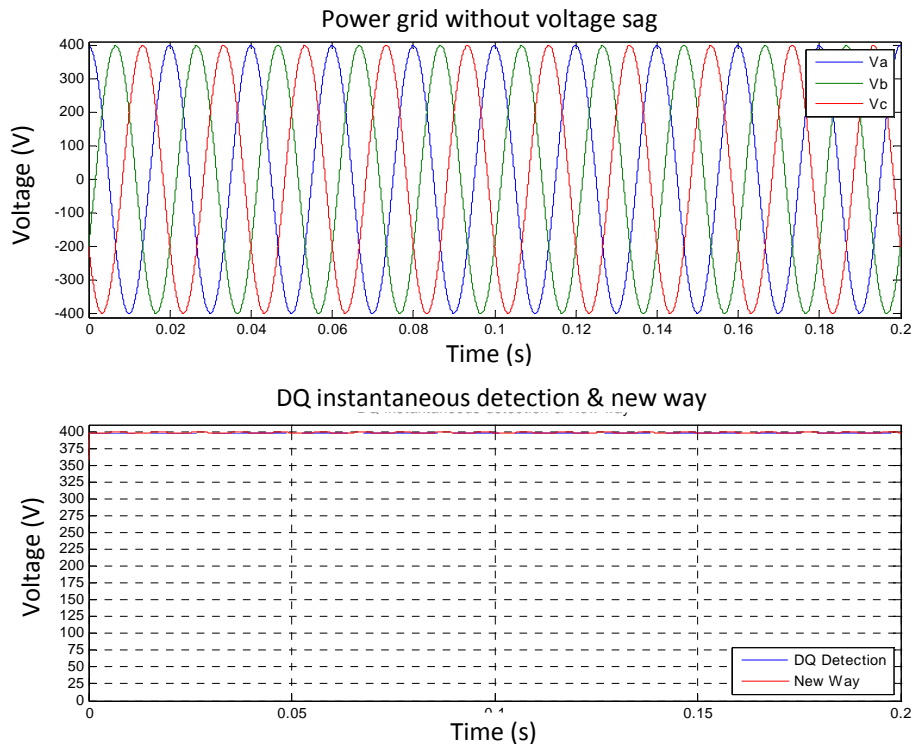


Figure 6- 8 Detection in the normal situation

Figure 6-9 illustrates the simulated result in accordance with the standard of Nordel grid code (Molinias Marta, et al. 2008). The power source for the simulation either falls or rises symmetrically. The simulated power source suddenly falls to 25% from 100% at 0.2s and maintains this value to 0.25s, then starts to linearly rise to 90% at 0.95s. Both the strategy DQ transform method and the new method work very well in this situation.

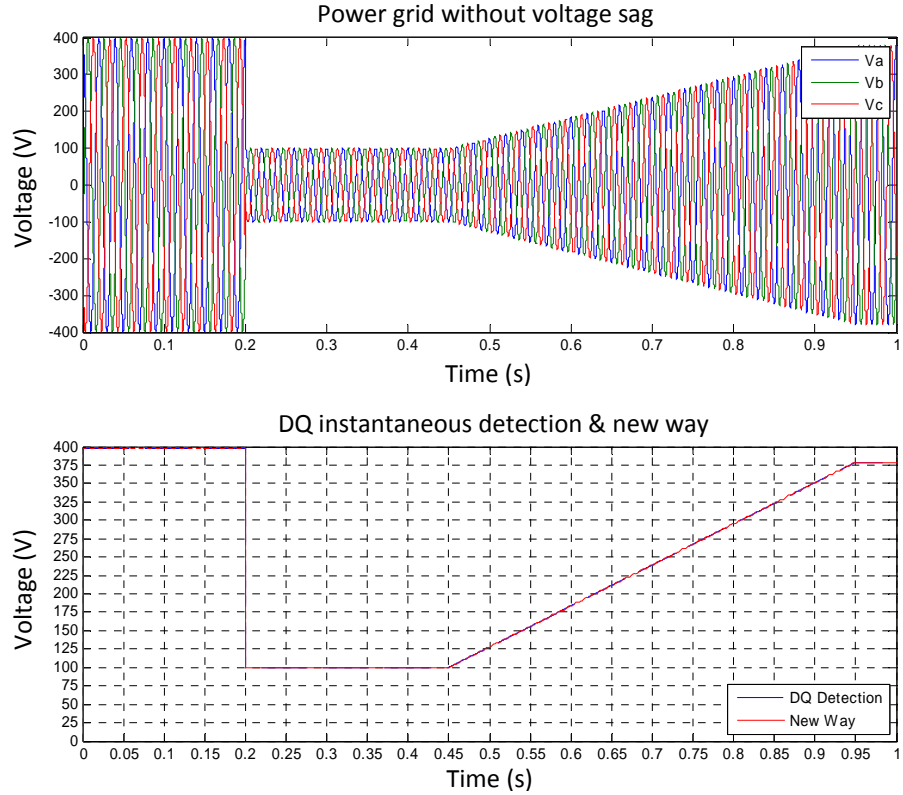


Figure 6-9 Nordel grid code

Figure 6-10 illustrates the German grid code (Shin H.J., et al. 2011), in this instance the simulated grid source falls down asymmetrically. Figure 6-10 shows the variation in the power source (top), the detection result obtained by the DQ transform (middle), this has oscillation. The bottom graph is achieved by means of the new method and is definitely consistent and accurate.

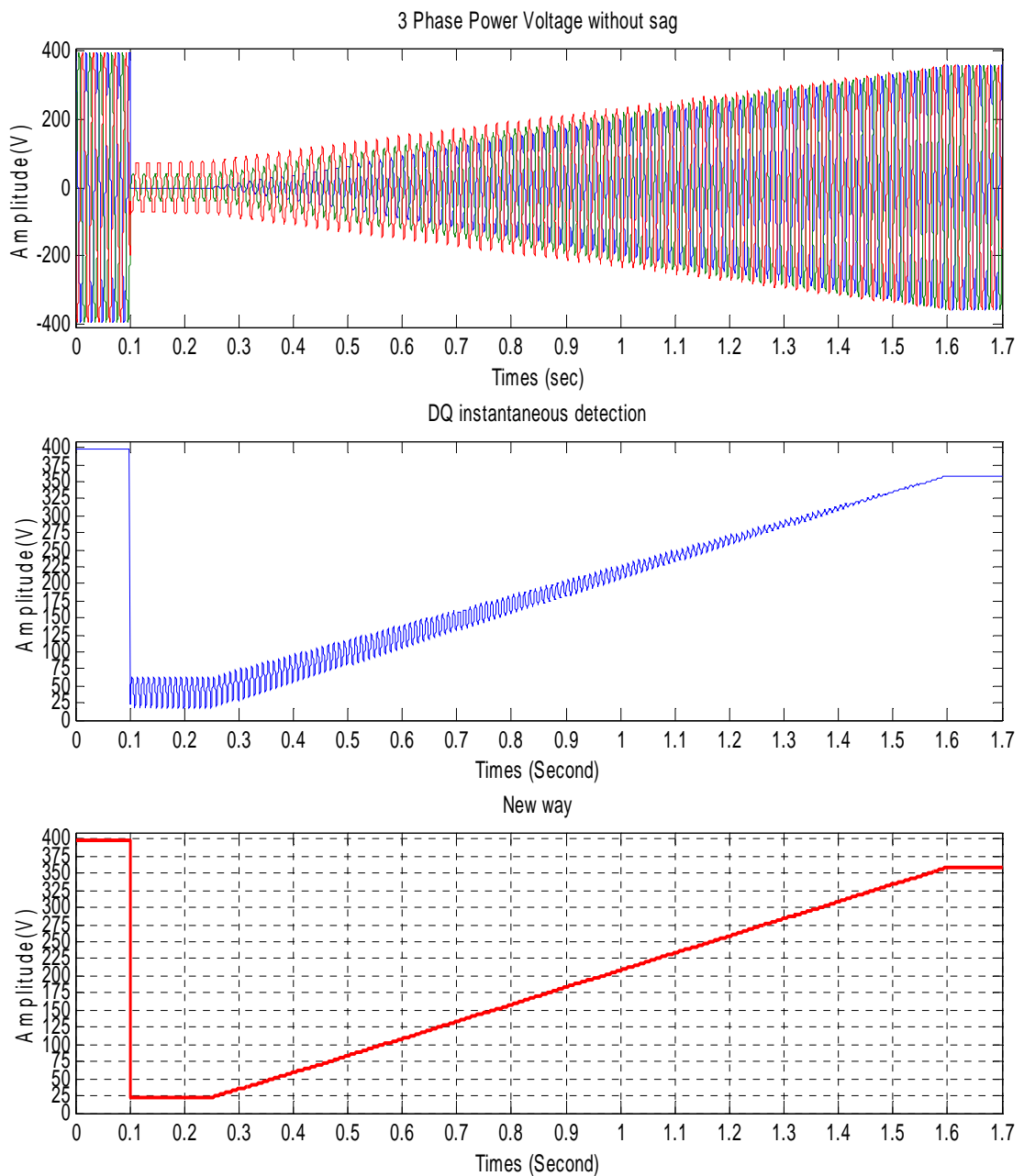


Figure 6- 10 German grid code

6.5 Summary

This chapter has discussed and compared several popular voltage sag detection methods, and analysed each method with their advantages and disadvantages.

The author developed an innovative algorithm for the 3-phase power grid voltage sag detection and the solution is simpler and more universal than other popular techniques.

To summarise by comparison of the detection results, if the voltage of the grid falls down either symmetrically or asymmetrically, the proposed new method is able to monitor and detect the changes in grid state with great clarity.

Chapter 7 Conclusion and Future Works

7.1 Conclusion

- In **Chapter 1**, the whole system framework is illustrated, clarifies the aim of project and describes objects which will be achieved in this project.
- In **Chapter 2**, an overview of the fundamental principles relating to wind turbines with grid connection is presented. It briefly summarises what technologies are currently employed in the development of the converter wind turbine, and the achievement made by this project.
- In **chapter 3**, the non-dimension characteristic of the power coefficient of a wind turbine as function of the tip speed ratio is, successfully obtained. A MATLAB model for a PMSG system was created and simulated to meet the specifications of a 10kW wind turbine, and the outcomes demonstrate that the model meets the design parameters.
- In **chapter4** demonstrates that the chosen diode rectifier with a boost circuit can be utilised for wind turbine generation with the generator voltage output less than that of the power grid. It means that this type of converter can be used in low wind speed conditions.
- In **chapter 5**, the results of simulations reveal that the SVPWM inverter have been completely achieved, includes a module for waveform sector identification, SVPWM carrier-wave and over-modulation.
- In **chapter 6**, the results of simulations prove that the proposed new detection method based on the DQ transform can rapidly monitor either symmetrical or asymmetrical voltage sag in the power grid.
- The context of chapter 6 has been accepted by *IEEE* conference, which will take place at Wuhan China in September.

7.2 Future works

- Although a successful model of PMSG has been created in Chapter 3, the wind turbine rotor torque is obtained from wind speed and the wind turbine rotor speed is obtained from the simulation. The model can be improved in terms of the input signal. For example, the current model only has a wind speed input.
- From the point of view of protection, the control system should consider the circumstance of over load or over current in the future.
- Chapter 4 solely concentrates on the feasibility of the diode rectifier following with a boost circuit for use in wind turbine system. The next step to consider is the improvement of the power factor of generator. This is the same issue for the inverter, to consider an improvement to the power qualities for grid.
- For the grid side inverter, the next step should consider how to inject the reactive power current into the grid for the purpose of stabilising the power grid.

References

1. Abbey, C. & Joos, G. 2005, Effect of low voltage ride through (LVRT) characteristic on voltage stability, IEEE Conference, pp. 1901-1907.
2. Ahmed T., Nishida K., & Nakaoka M. 2004, Wind Energy DC Supply-Based Induction Generator with Static VAR Compensator and AC Voltage Regulator, *In INTELEC 2004, 26th Annual International*, IEEE, pp. 689-696.
3. Alepuz S., Calle A., Busquets-Monge S., Bordonau J., Kouro S., & Wu B. 2010, Control Scheme for Low Voltage Ride-Through Compliance in Back-to-Back NPC Converter Based Wind Power Systems, *In 2010 IEEE International Symposium on*, IEEE, pp. 2357-2362.
4. Anaya-Lara O., Jenkins N., Ekanayake J., Cartwright P., & Hughes M. 2009a, "Doubly Fed Induction Generator (DFIG)-based Wind Turbines," *In Wind Energy Generation: Modelling and Control*, First ed. John Wiley & Sons, Ltd, pp. 77-97.
5. Anaya-Lara O., Jenkins N., Ekanayake J., Cartwright P., & Hughes M. 2009b, "Electricity Generation from Wind Energy," *In Wind Energy Generation: Modelling and Control*, First ed. John Wiley & Sons, Ltd, pp. 1-18.
6. Arroyo E.L.C. 2006. *Modeling and Simulation of Permanent Magnet Synchronous Motor Drive System*.
7. Belakehal S., Benalla H., & Bentounsi A. 2009. Power Maximumization Control of Small Wind System Using Permanent Magnet Synchronous Generator. *Revue des Energies Renouvelables*, 12, (2) 307-319
8. Bharanikumar R., Yazhini A.C., & Kumar A.N. 2010. Modeling and Simulation of Wind Turbine Driven Permanent Magnet Generator with New MPPT. *Asian Power Electronics Journal*, Vol. 4, (2) 52-58
9. Borowy Bogdan S. & Salameh Ziyad M. 1997. Dynamic Response of a Stand-Alone Wind Energy Conversion System with Battery Energy Storage to a Wind Gust. *IEEE Transactions on Energy Conversion*, 12, (1) 73-78
10. Burton T., Sharpe D., Jenkins N., & Bossanyi E. 2001, "Introduction," *In Wind Energy Handbook*, John Wiley & Sons, Ltd, pp. 1-10.
11. Busca C., Stan A., Stanciu T., & Stroe D.I. 2010, Control of Permanent Magnet Synchronous Generator for Large Wind Turbines, *In 2010 IEEE International Symposium on*, IEEE, pp. 3871-3876.
12. BWEA 2009, *Annual Review 2009*, British Wind Energy Association.
13. Chi Y.N. 2009, *Comparison of LVRT requirements worldwide - Why do we need LVRT?*, China Electric Power Research Institute.

14. Chu H.Y., Jou H.L., & Huang C.L. 1992. Transient Response of a peak Voltage Detector for Sinusoidal Signals. *IEEE Transactions on Industry Electronics*, 39, (1) 74-79
15. Czarkowski D. 2001, "DC-DC Converters," *In Power Electronics Handbook*, Rashid M.H., ed., Oxford University Press, pp. 245-259.
16. Deckmann S.M. & Ferrira A.A. 2002, About Voltage Sags and Swells Analysis, *In 2002. 10th International Conference on*, IEEE, pp. 144-148.
17. Depenbrock M. 1988. Direct Self-Control (DSC) of Inverter-Fed Induction Machine. *IEEE Transactions on power electronics*, 3, (4) 420-429
18. Ding K., Cheng K.W.E., Xue X.D., Divakar B.P., Xu C.D., Che Y.B., Wang D.H., & Dong P. 2006, A Novel Detection Method for Voltage Sags, *In 2006 ICPESA 2nd International Conference on Power Electronics Systems and Applications*, IEEE, pp. 250-255.
19. Espinoza J.R. 2001, "Inverters," *In Power Electronics Handbook*, Rashid M.H., ed., Oxford University Press, pp. 353-404.
20. Fitzer C., Barnes M., & Green P. 2004. Voltage Sag Detection Technique for a Dynamic Voltage Restorer. *IEEE Transactions on industry applications*, 40, (1) 203-212
21. Hau Erich 2006, "Physical Principles of Wind Energy Conversion," *In Wind Turbines: Fundamentals, Technologies, Application, Economics*, pp. 81-90.
22. Henryk Markiewicz & Antoni Klajn. 2004, Voltage Disturbances Standard EN50160 - Voltage Characteristic in Public Distribution Systems.
23. Horizon Gitano-Briggs 2010, "Small Wind Turbine Power Controllers," *In Wind Power*, pp. 165-188.
24. Johnson C.C. & Smith Richard T. 1976. Dynamics of Wind Generators on Electric Utility Networks. *IEEE Transactions on Aerospace and Electronic Systems*, AES-12, No. 4, 483-493
25. Johnson G.L. 2006, "Wind Turbine Power, Energy, and Torque," *In Wind Energy System*, Electrical Edition ed. Prentice-Hall Englewood Cliffs (NJ), pp. 4-1-4-54.
26. Kirtley J.L. 2010, "Polyphase Systems," *In Electric Power Principles: sources, conversion, distribution and use*, First ed. John Wiley & Sons, Ltd, pp. 45-56.
27. Lee Chia-Tse, Hsu Che-Wei, & Cheng Po-Tai 2011. A Low-Voltage Ride-Through Technique for Grid-Connected Converters of Distributed Energy Resources. *IEEE Transactions on industry applications*, 47, (4) 1821-1832
28. Li S.H., Haskew T.A., Swatloski R.P., & Gathings W. 2012. Optimal and Direct-Current Vector Control of Direct-Driven PMSG Wind Turbines. *IEEE Transactions on power electronics*, 27, (5) 2325-2337

29. Meziane R.T.S. & Benalla H. 2007. Direct torque control for induction motor using intelligent techniques. *Journal of Theoretical and Applied Information Technology*, 3, (3) 35-44
30. Cai Mingfa 2006, *The AC Motor Control Simulation and the Construction of an SVPWM Block via Simulink.*
31. Molinas Marta, Jon Are Suul, & Undeland Tore 2008. Low Voltage Ride Through of Wind Farms With Cage Generators: STATCOM Versus SVC. *IEEE Transactions on power electronics*, 23, (3) 1104-1117
32. Quang N.P. & Dittrich J.A. 2008, "Inverter control with space vector modulation," *In Vector Control of Three-Phase AC Machines*, First ed. Springer, pp. 17-59.
33. Wang Quincy & Chang Liuchen 2004. An Intelligent Maximum Power Extraction Algorithm for Inverter-Based Variable Speed Wind Turbine Systems. *IEEE Transactions on power electronics*, 19, (5) 1242-1249
34. Bana Sharifian M.B, Mohamadrezapour Y., Hosseinpour M., & Torabzade S. 2009. Maximum Power Control of Variable Speed Wind Turbine Connected to Permanent Magnet Synchronous Generator Using Chopper Equipped with Superconductive Inductor. *Journal of Applied Sciences*, 9, (4) 777-782
35. Shaw S.R. & Leeb S.B. 1999. Identification of induction motor parameters from transient stator current measurements. *IEEE Transactions on Industrial Electronics*, 46, (1) 139-149
36. Shin H.J., Jung H.S., & Sul S.K. 2011, Low Voltage Ride Through Control Strategy of Grid-connected Variable Speed Wind Turbine Generator System, *In 2011 IEEE Power Electronics and ECCE Asia 8th International Conference*, IEEE, pp. 96-101.
37. Takahashi Isao & Noguchi Toshihiko 1986. A New Quick-Response and High-Efficiency Control Strategy of an Induction Motor. *IEEE Transactions on industry applications*, IA-22, (5) 820-827
38. Texas Instruments 1997, *Clarke & Park Transforms on the TMS320C2xx*, Texas Instruments, BPRA048.
39. Yang W.R. & Yang W.X. 2010, Discrete Wavelet Transform and Short-Time Fourier Transform Applications: Wafer Microcrack and Voltage Sag Detection, *In 2010 International Conference on System Science and Engineering (ICSSE)*, IEEE, pp. 31-35.
40. Zhou M.X., Bao G.Q., & Gong Y. 2011, Maximum Power Point Tracking Strategy for Direct-Driven PMSG, *In 2011 Asia-Pacific Power and Energy Engineering Conference (APPEEC)*, IEEE, pp. 1-4.

Appendix-A 10kW case study wind turbine specification

Parameters	Unit	Value
Rated power	Watts	10000
Rated wind speed	m/s	8.5
Aiming start wind speed	m/s	2.9
Aiming cut-in wind speed	m/s	3.2
Cut-out wind speed	m/s	16
Air density	kg/m ³	1.225
Number of blades	-	3
Design tip speed ratio	-	8
Rotor radius	m	5
Generator poles	-	24
Generator synchronizing frequency	Hz	26
Gear ratio	-	N/A
Rotor aerodynamic power coefficient Cp at rated wind speed		0.43
Total power coefficient at rated wind speed	-	0.3385
Designed rotor speed	RPM	130
Design generator speed	RPM	130

Appendix-B C_p vs λ

```
%Simulation of the wind turbine power Output
close all,clear all,clc;
%-----
%Definition the radius of wind turbine
% 5 meter
%-----
radius=5;
%-----
%Define the total efficiency of wind turbine
%-----
TotalEfficiency = 0.7872;
%The density of air at sea level 1.225 kg/m^3
%-----
densAir=1.225;
%-----
%Define the rang of wind velocity: 4.5m/sec--9m/sec
%-----
MinVelocity=4.5;
MaxVelocity=9;
%-----
%Define rotor speed from 3/rps to 80 rps
%-----
MinOmega=3;
MaxOmega=80;
%-----
%
%-----
Step=0.1;
Velocity=MinVelocity:0.5:MaxVelocity;
Omega=MinOmega:Step:MaxOmega;
m=length(Velocity);
n=length(Omega);
Lambda=zeros(m,n);
%-----
%Determine all of lambda
%-----
for i=1:m
    v=Velocity(i);
    for j=1:n
        Lambda(i,j)=radius*Omega(j)/v;
    end
end
%-----
%To calculate wind turbines coefficient performance Cp
%-----
Cp1=0.052;
Cp2=0.118;
Cp3=0.16;
Cp4=0.062;
Cp5=1.026e-2;
Cp6=5.65e-4;
Cp=zeros(m,n);
for i=1:m
    for j=1:n
        Lamd=Lambda(i,j);
        Cp(i,j)=Cp1-Cp2*Lamd+Cp3*Lamd^2-Cp4*Lamd^3 ...
    end
end
```

```

        +Cp5*Lamd^4-Cp6*Lamd^5;
    if(Cp(i,j)<0)
        Cp(i,j)=0;
    end
    Cp(i,j)=Cp(i,j)*0.7*0.558;
end
end
%-----
%
%-----
Power=zeros(m,n);
for i=1:m
    v=Velocity(i);
    Power(i,:)=TotalEfficiency*0.5*Cp(i,:)*densAir*pi*(radius^2)*(v^3);
end
%%
scrsz = get(0,'ScreenSize');
%-----
%Plot turbine power output versus rotor speed
%-----
ZeroPosition=find(Cp(m,:)==0);
if(isempty(ZeroPosition))
    Len=n;
else
    Len=ZeroPosition-1;
end
figure('position',[50 50 scrsz(3)/2-100 scrsz(4)/2-100]);
plot(Omega(:,1:Len),Power(:,1:Len));
hold on;

title('Turbine output power versus rotor speed');
xlabel('Rotor Speed in Second (rad/s)');
ylabel('Power output in Watt (w)');
%%
%-----
%Plot turbine maximum power output curve
%-----
MaxPower=zeros(1,m);
Position=zeros(1,m);
MaxValue=1e-6;
J=0;
for i=1:m
    MaxPower(i)=max(Power(i,:));
    MaxValue=max(Power(i,:));
    J=find(Power(i,:)==MaxValue);
    Position(i)=J*Step+MinOmega;
end
plot(Position,MaxPower,'--.r');
hold off;
%%
%-----
%Label marks for every curve
%-----
str1='V=';
str3=' m/sec';
for i=1:m/2
    str2=num2str(i+3+0.5);
    str=strcat(str1,str2);
    text(Position((i-1)*2+1),MaxPower((i-1)*2+1),str);
    str2=num2str(i+3+1);
    str=strcat(str1,str2);
    text(Position(i*2),MaxPower(i*2),str);
end

```

```

%%
%-----%
%Plot Power coefficient versus Tip speed rotor
%-----%
ZeroPosition=find(Cp(1,:)==0);
if isempty(ZeroPosition)
    Len=n;
else
    Len=ZeroPosition-1;
end
figure('position',[scrsz(3)/2 50 scrsz(3)/2-100 scrsz(4)/2-100]);
plot(Lambda(1,1:Len),Cp(1,1:Len));
title('Power Coefficient VS Tip speed ratio');
xlabel('Lambda');
ylabel('Cp');
grid on;
%%

```

Appendix-C PMSG parameters

```
%-----  
%Definition the radius of wind turbine  
%-----  
radian=5;  
%-----  
%Define permanent magnet flux linkage amplitude 1.02V/s  
%-----  
LambdaM=6.415;  
%-----  
%The density of air at sea level 1.225 kg/m^3  
%-----  
densAir=1.225;  
%-----  
% The frequency of voltage output from generator  
%-----  
Frequency=26;  
Period=1/Frequency;  
%-----  
%Define the coefficients for calculate power coefficient  
%-----  
Cp=0.3385;  
% -----  
%Define the length of the strongly disturbed  
%airstream of upwind and downwind of the rotor  
%In order to extract maximum wind energy, it's suggested  
%s is equal to half-length of blade r  
%s=0.5*radian  
% -----  
s=0.5*radian;  
%-----  
%Define number of blade  
%-----  
n=3;  
%-----  
%To observe the coefficient of rotor  
%Omega=2*pi*V/(n*s)  
%-----  
OmegaCoeff=2*pi/(n*s);  
%-----  
% Define the gear ratio  
%-----  
GRatio = 1;  
%-----  
% Define the Direct axis stator inductance Ld, H  
%-----  
Ld = 0.05;  
%-----  
% Define the Quadrature axis stator inductance Lq, H  
%-----  
Lq = 0.05;  
%-----  
% Define stator phase winding resistance, Ohm  
%-----  
Rs = 5;
```

```

%-----
% Define the poles of turbine
%-----
Poles = 24;
%-----
% Define the moment of inertia referred to the
% shaft of the generator, kgm^2
%-----
Jg = 3;
%-----
% To obtain coefficient of the voltage angular
% velocity of generator
%      W = 2*Wr/(Poles*GRatio);
% where
%      W is the mechanical angular velocity in rps
%      Wr is the rotor angular velocity of the generator
%      Poles is the number of poles on the rotor
%
%      Wr=W*[ (Poles*GRation)/2]
%      Coefficient of the rotor angular velocity of the
%      generator can be expressed:
%      (Poles*GRation)/2
%-----
CoeffPowerOmega = (Poles*GRatio)/2;

```

Appendix-D C Program for S-Builder filter

```
static double NewSample=0;
static double OldSample=0;
static double Output=0;
static int Count=0;

NewSample=u[0];
if(NewSample==OldSample)
{
    Count++;
    if(Count++>=3)
    {
        Output=OldSample;
        Count=0;
    }
}
else
    Count=0;
OldSample=NewSample;
y[0]=Output;
```